Covert Performance of STAR-RIS Aided THz Communication System with RSMA and Phase Errors

Xiangbin Yu, *Senior Member, IEEE*, Yue Zhou, Shihao Yan, *Senior Member, IEEE*, Yun Rui, *Senior Member, IEEE*, Xiaoyu Dang, Chau Yuen, *Fellow, IEEE*, Mohsen Guizani, *Fellow, IEEE*

***Abstract*—In this paper, the covert performance of the simultaneous transmitting and reflecting reconfigurable intelligent surface (STAR-RIS) aided Terahertz (THz) communication systems with rate-splitting multiple access (RSMA) over the generalized α-μ fading channel is studied, where the discrete phase error and noise power uncertainty are considered. By means of the Gaussian approximation and Gamma distribution, the closed-form outage probability (OP) of the legitimate users is firstly derived. Then, the covert performance of the system is analyzed, and average detection error probability (ADEP) is deduced for the warden, and resultant closed-form ADEP is obtained. By minimizing the ADEP, the optimal detection threshold is derived with closed-form expression. With these results, subject to the constraints of covertness and reliability, the power allocation (PA) coefficients are optimized to minimize the OP of the covert user. Two adaptive PA schemes based on two-dimensional (2D) and one-dimensional (1D) search methods are respectively proposed to achieve the solutions, and resulting lower OP is attained. Simulation results indicate that the theoretical OP and ADEP can agree the corresponding simulations well, and randomizing the noise power of warden can improve the covert performance. Moreover, the warden with the optimized threshold can obtain lower ADEP than that with a fixed threshold, and the system with two PA schemes has a lower OP than that with a fixed PA, especially the scheme based on 1D search has lower complexity while maintaining the superior performance.**

***Index Terms*—Covert communication, THz communication, RSMA, detection error probability, outage probability, phase error, noise power uncertainty.**

I. INTRODUCTION

In the era of rapid technological advancement, the demand for high-speed, high-quality communication has spurred research into the sixth-generation (6G) mobile communication technology. As one of the key technologies in 6G networks, terahertz (THz) communication, which utilizes high-frequency THz waves for information transmission, can offer broad bandwidth, high speed, and low latency, effectively addressing the spectrum resource scarcity faced by the fifth-generation (5G) mobile communication [1]. However, the transmission distance is limited due to the high-frequency characteristics of THz waves. This limitation can be mitigated by the reconfigurable intelligent surface (RIS) [2] [3] and integrating simultaneous transmitting and reflecting RIS (STAR-RIS) [4] techniques, which enhance the signal coverage and optimize the propagation paths, thus improving system performance.

As an improvement of conventional RIS, STAR-RIS not only splits the received wireless signals into the transmitted and reflected components for propagation to both sides of the surface, enabling full-space reconfigurable wireless environments, but also eliminates the requirement for transmitters and receivers to be on the same side of the surface, significantly enhancing the channel quality and coverage of the communication system [5]. However, managing interference between the transmitted and reflected users remains a critical challenge in applying STAR-RIS to multiuser communication scenarios. Rate-splitting multiple access (RSMA), as a promising multiple access technique in 6G communication, has high spectrum efficiency, enables dynamic resource allocation and allows multiple users to share the same communication channel while maintaining their respective data transmission rates. Thus, it can offer the flexibility and high efficiency [6].

Recently, covert communication technique has received much attention since it can offer to protect the privacy and security of served users. In covert communication, information must be hidden within irrelevant data to avoid detection and interference by the wardens, ensuring minimal probability of discovery by the monitors while guaranteeing successful decoding by the intended receiver [7] [8]. The covert communication combined with RIS technology can provide an effective covert approach, i.e., leveraging the RIS's adjustable reflection properties to optimize signal propagation paths, enhance signal penetration and coverage, and improve the robustness of covert communication. Moreover, RIS's signal reconfiguration capabilities further enhance the security and reliability of covert communication [9] [10]. Besides, using the RIS technique can also improve the physical layer security of the communication systems [11]–[13]. The spatial secrecy spectral efficiency (SE) optimization enabled by RIS for MISO system was investigated in [11], a joint design of the transmit digital beamforming and the RIS analog phase profile based on the alternating optimization and minorization-maximization methods was presented to improve the secrecy SE. In [12], a physical layer security scheme that jointly designs the

This work was supported in part by Natural Science Foundation of China (62031017, 62471228).

X.Yu, Y. Zhou are with the College of Electronic and Information Engineering, Nanjing University of Aeronautics and Astronautics, Nanjing, China (e-mail: yxbxwy@gmail.com). S. Yan is with the School of Science, Edith Cowan University, Perth, WA 6027, Australia. Y. Rui is with the School of Communication and Electronic Engineering, East China Normal University, Shanghai, China. X. Dang is with Space Information Research Institute, Hangzhou Dianzi University. C. Yuen is with School of Electrical and Electronics Engineering, Nanyang Technological University, Singapore. M. Guizani is with Mohamed Bin Zayed University of Artificial Intelligence, Abu Dhabi, UAE.

legitimate precoding matrix and the artificial noise covariance matrix, as well as the legitimate combining matrix and the reflection coefficients of the legitimate RIS was developed for MIMO system to improve the secrecy rate performance. A novel RIS-aided privadcy-preserving integrated sensing and communications scheme was presented in [13], where the RIS phase configuration was designed to maximize the users' sum rate and minimize the projection of the wiretapper's effective channel onto the legitimate channel.

By introducing STAR-RIS in covert communication, i.e., STAR-RIS aided covert communication, some studies have demonstrated the effectiveness of their integration [14] - [16]. In [14], STAR-RIS assisted covert multicasting was investigated, which considered the hardware impairments and two distinct STAR-RIS protocols, and the covert rate was maximized by optimizing parameters under both perfect and imperfect wiretap channel state information. A STAR-RIS aided covert communication system was explored in [15], where a full-duplex receiver emitted jamming signals to disrupt the wardens. The minimum detection error probability (DEP) problem at the warden was formulated, and an iterative algorithm was presented to solve the non-convex optimization problem. The authors in [16] examined the impact of large-scale deployment of STAR-RIS on covert communication, leveraging its unpredictability to enhance covertness, where the average DEP (ADEP) was derived, and the covert rates were maximized by optimizing the passive beamforming.

Combined with different multiple access schemes, the covert performance of STAR-RIS-aided system can be improved. In [17], the performance of STAR-RIS-aided non-orthogonal multiple access (NOMA) systems with imperfect successive interference cancelation (SIC) was studied, where the DEP, detection threshold, and average DEP were derived for evaluation. A covert communication scheme for STAR-RIS-assisted NOMA networks in Nakagami-*m* fading channels was proposed in [18], where Kullback-Leibler divergence was used to analyze the warden's detection performance, and closed-form expressions for some performance metrics were provided. In [19], the authors investigated the covert and secrecy performances of a STAR-RIS-assisted uplink NOMA system with semi-grant-free transmission under illegal user, where the outage probability (OP), DEP, and secrecy OP were respectively deduced to evaluate the system performances. Besides, the integration of RSMA with STAR-RIS can improve the interference management and system flexibility. The authors in [20] studied an intelligent autonomous transport system combining STAR-RIS with RSMA (STAR-RIS-RSMA) to improve the communication security and covertness, where the system reliability, covertness and security were evaluated in the presence of eavesdropping vehicles and roadside devices. Authors in [21] presented a covert communication scheme for STAR-RIS-RSMA networks, optimizing the full-duplex receiver's jamming signals and STAR-RIS's reflection coefficients to enhance the covert performance. In [22], the covert communications for STAR-RIS-RSMA assisted ambient backscatter communication system was investigated. With the performance analysis, the expressions of DEP, OP, covert rate and SE were derived for the assessment, and the impact of different system parameters on the performance was analyzed. An active STAR-RIS-RSMA system was investigated in [23], where the OP, DEP and covert transmission rates were analyzed and deduced for the evaluation. Considering the performance analysis above is based on the conventional microwave band, the covert communication in THz band was studied in [24] [25]. Authors in [24] presented a unmanned aerial vehicle (UAV)-mounted RIS-aided THz communication system, which leveraged the RIS for reliable transmission and additional UAVs to generate artificial noise for enhanced covertness. In [25], a distance-adaptive absorption peak modulation for THz covert communication was proposed, and it can reduce the monitor range and improve security for THz covert communication.

According to the literature survey above, the covert performance for STAR-RIS/STAR-RIS-RSMA communication systems has been investigated, but it is basically based on the conventional microwave band, while the related work on the THz communication system is less studied, especially in the presence of the discrete phase errors, noise power uncertainty and the generalized α -μ channel. To the best of our knowledge, the performance of STAR-RIS aided THz systems with RSMA (THz-RSMA) over the α -μ fading channel is not studied. In practice, the phase errors will be unavoidable due to the limited number of phase shifts [26] [27]. Besides, the more general composite THz channel including small-scale α -μ fading and large-scale molecular absorption effects is not considered. It is of practical significance to take the discrete phase errors and generalized α -μ channel into account when analyzing the covert performance of STAR-RIS aided THz-RSMA systems.

Motivated by the reasons above, we will study the covert performance of STAR-RIS aided THz-RSMA over the generalized α-μ fading channel. The OP and ADEP are respectively derived for the covert performance evaluation and optimization. With these results, the optimal detection threshold is derived to minimize the ADEP, and the power allocation (PA) coefficient is optimized to minimize the OP. The main contributions of this paper are summarized as follows:

1) The STAR-RIS aided THz-RSMA system with phase errors is firstly presented. Based on this model, the covert performance of the system with phase errors and noise power uncertainty over the generalized α-μ fading channel is investigated and optimized. The outage probabilities of two legitimate users (Bob and Carl) are respectively derived for the performance analysis, and resultant closed-form expressions are attained, which will benefit the performance evaluation and optimization.

2) The covert performance of STAR-RIS aided THz-RSMA system is then analyzed, and the closed-form expressions of the ADEP for the warden Willie is derived for performance evaluation and optimization, where the noise power of warden is randomized and is subject to a uniform distribution. Based on this, an optimal detection threshold is derived by minimizing the ADEP. As a result, the closed-form optimal threshold and ADEP are attained. Meanwhile, the asymptotic ADEP at high power is derived. It is interestingly found that this asymptotic ADEP is only related to the PA coefficient

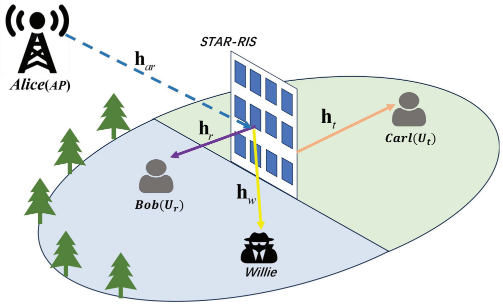

Fig. 1. STAR-RIS aided THz-RSMA communication system.

of covert user, and is also a decreasing function on this PA coefficient. Thus, the covert performance can be increased by decreasing this coefficient under high power. Besides, the noise power uncertainty also brings the increase of covertness.

3) Under the constraints of the target OP and covertness, the PA coefficients are designed for minimizing the OP of the covert user, and an optimal PA scheme based on two-dimensional (2D) search method is proposed to obtain the solution. To reduce the complexity, a suboptimal PA scheme based on one-dimensional (1D) search method is also presented, and it has the performance close to that of the optimal scheme but with low complexity. Simulation results show that the presented theoretical analysis is valid and matches the simulations well. Moreover, the system with the proposed optimal detection threshold can obtain lower ADEP than that with the conventional fixed threshold. Besides, the system with the proposed two PA coefficients can achieve superior outage performance over that with the fixed one.

Notations: $\mathcal{CN}(a,b)$ denotes complex Gaussian distribution, whose expectation is a and variance is b. $\angle h$ denotes the phase of complex number h. $\mathrm{U}(c,d)$ means taking the uniform distribution over the interval $[c,d]$, $\mathcal{N}(a,b)$ denotes the Gaussian distribution with mean a and variance b.

The remainder of the paper is organized as follows. Section II presents the system model for a STAR-RIS assisted THz communication system with RSMA and phase errors, where the signal-to-noise ratio (SINR) is deduced for the performance analysis. In Section III, the outage performance of the system is analyzed, and the closed-form OP is derived. The covert performance analysis is presented in Section IV, where the ADEP is deduced for the evaluation. In Section V, two adaptive PA schemes are developed to minimize the OP, and the corresponding algorithm realizations are also presented. Simulation results are offered in Section VI. Section VII summarizes the main conclusions.

II. System model

We consider a STAR-RIS assisted THz-RSMA system, which consists of one single-antenna access point (AP), one STAR-RIS, two single-antenna legitimate users and a warden. The legitimate users are Bob (U_r) and Carl (U_t), legitimate transmitter is Alice, and the warden is Willie. The STAR-RIS is composed of M passive elements. U_r and U_t are distributed in the reflection and transmission regions of STAR-RIS, respectively. The direct channels between the AP and the users are blocked due to the obstacles. The STAR-RIS aided THz-RSMA system model is shown in Figure 1.

A. Channel Model

In this paper, we consider a THz channel, which is modeled as composite fading channel including large-scale path loss and small-scale $\alpha{-}\mu$ fading. The channels between the AP and STAR-RIS, between STAR-RIS and the legitimate users, and between STAR-RIS and Willie are denoted by $\mathbf{h}_p \in \mathbb{C}^{M\times 1}$, $p \in \{ar, t, r, w\}$. The m-th element in $\mathbf{h}_p$ is expressed as $h_{p,m}$, $h_{p,m} = \bar{h}_p \tilde{h}_{p,m}$, where $\tilde{h}_{p,m}$ represents the small-scale fading, $\bar{h}_p$ represents the path loss and it consists of the path loss and molecular absorption loss, which is modeled as [28]

$$\bar{h}_p = \frac{c\sqrt{G_t G_r}}{4\pi f d_p} \exp\left(-\frac{1}{2}\kappa_{\tilde{\alpha}}(f)\, d_p\right), \tag{1}$$

where G_t and G_r represent the antenna gains at the transmitter and receiver, respectively. c is the speed of light and f is the operating frequency. $\kappa_{\tilde{\alpha}}(f)$ is the molecular absorption coefficient, which indicates the amount of energy that the molecules of the medium absorb from the electromagnetic wave and is related to relative humidity, atmospheric pressure and temperature. d_p denotes the distance from STAR-RIS to the legitimate users or to Willie.

The small-scale fading $\tilde{h}_{p,m}$ is modeled as a random variable of $\alpha - \mu$ [28], [29], and its probability density function (PDF) can be expressed as [28]

$$f_{|\tilde{h}_{p,m}|}(x) = \frac{\alpha \varrho^{\alpha\mu} x^{\alpha\mu - 1}}{\hat{h}_f^{\alpha\mu}\Gamma(\mu)} \exp\left(-\varrho \frac{x^\alpha}{\hat{h}_f^\alpha}\right), \tag{2}$$

where $\varrho = \frac{\Gamma(\mu + 1/\alpha)}{\Gamma(\mu)}$, α is the fading parameter, μ is the normalized variance of fading channel envelope, and $\hat{h}_f$ is α-root mean value of channel envelope. $\Gamma(\cdot)$ is the gamma function [30]. When $\alpha = 2$ and $\mu = m$, the $\alpha - \mu$ channel is reduced to the conventional Nakagami-m channel, and when $\alpha = 2$ and $\mu = 1$, it is reduced to the conventional Rayleigh channel [28].

B. Signal Transmission

According to the principle of STAR-RIS scheme [31], the signal is transmitted through the STAR-RIS reflection module to U_r and through the transmission module to U_t. Compared to conventional RIS, the STAR-RIS can improve the coverage to 360^o, which obviously increases the communication range. In terms of [31], the coefficient matrix of STAR-RIS can be given by

$$\mathbf{\Theta}_k = \sqrt{\beta_k}\mathrm{diag}\left(e^{j\varphi_{k,1}}, \ldots, e^{j\varphi_{k,M}}\right), \;\; k \in \{t, r\}, \tag{3}$$

where β_t and β_r are respectively transmission and reflection amplitude coefficients of STAR-RIS elements, satisfying $\beta_t + \beta_r = 1$, $0 \le \beta_k \le 1$. $\varphi_{k,m} \in [0, 2\pi)$ for $m \in \{1, 2, \ldots, M\}$ is the phase shift of the m-th element of the STAR-RIS, and it can be designed as $\varphi^*_{k,m} = \angle h_{k,m} - \angle h_{ar,m}$ to obtain the maximal received signal power [31]. Considering that perfect phase matching is hard to achieve due to a limited set of discrete phases in practice [26] [27], the coefficient matrix can be re-expressed as

$$\tilde{\mathbf{\Theta}}_k = \sqrt{\beta_k}\text{diag}\left(e^{j\tilde{\varphi}_{k,1}}, \ldots, e^{j\tilde{\varphi}_{k,M}}\right), \tag{4}$$

where $\tilde{\varphi}_{k,m} = \varphi^*_{k,m} + \bar{\varphi}_{k,m}$ is the phase shift after the introduction of phase quantization error for the *m*-th element of STAR-RIS, $\bar{\varphi}_{k,m}$ is the discrete phase error of the *m*-th element. It follows an uniform distribution [26] [27], i.e., $\bar{\varphi}_{k,m} \sim \mathrm{U}(-\upsilon\pi, \upsilon\pi)$, and $\upsilon = \frac{1}{2^b} \in (0, 1]$, where b is number of quantization bits [26].

In a RSMA-assisted communication system, all common messages are encoded into a single common stream that must be decoded by all users. Meanwhile, private messages are individually encoded into separate private streams, each intended for its corresponding receiver. By splitting the information into private and common components, RSMA optimizes the spectrum utilization, particularly in scenarios where interference exists between users. This approach allows for more efficient use of available bandwidth. According to the RSMA transmission protocol, the transmitting signals at the AP are

$$x_1[i] = \sqrt{P_s}\left(\sqrt{a_c}s_c[i] + \sqrt{a_t}s_t[i] + \sqrt{a_r}s_r[i]\right), \tag{5}$$

where $i = 1, \ldots, I$ is the i-th time slot and I denotes the total number of time slots. P_s is the transmit power of the AP, a_c is the PA coefficient for transmitting the public message, a_k is the PA coefficient for transmitting the private message to user U_k and satisfies $a_c + a_t + a_r = 1$. The received signal at user U_k is denoted as

$$y_k[i] = \mathbf{h}_k^H \tilde{\mathbf{\Theta}}_k \mathbf{h}_{ar} x_1[i] + n_k[i], \tag{6}$$

where $n_k[i]$ is the Gaussian white noise at the user end and satisfies $n_k[i] \sim \mathcal{CN}\left(0, \sigma_k^2\right)$. Assume that the noise power at legitimate user k is equal, i.e. $\sigma_0^2 = \sigma_k^2$.

For the RSMA system, the legitimate user U_k decodes the common information firstly and treats all private information as interference, thus the SINR for the common information is

$$\gamma_{c,k} = \frac{a_c P_s \left|\mathbf{h}_k^H \tilde{\mathbf{\Theta}}_k \mathbf{h}_{ar}\right|^2}{(a_k + a_{\bar{k}}) P_s \left|\mathbf{h}_k^H \tilde{\mathbf{\Theta}}_k \mathbf{h}_{ar}\right|^2 + \sigma_0^2}. \tag{7}$$

After performing SIC via removing the interference caused by the common information signals, the SINR for U_k to decode its private information is

$$\gamma_{p,k} = \frac{a_k P_s \left|\mathbf{h}_k^H \tilde{\mathbf{\Theta}}_k \mathbf{h}_{ar}\right|^2}{a_{\bar{k}} P_s \left|\mathbf{h}_k^H \tilde{\mathbf{\Theta}}_k \mathbf{h}_{ar}\right|^2 + \sigma_0^2}, \tag{8}$$

in which $\bar{k} = \{t, r\}$. When $k = t$, we have $\bar{k} = r$, and vice versa.

III. Outage performance analysis

In this section, we analyze the outage performance of legitimate users in the presence of the STAR-RIS phase errors, and derive the OP for obtaining the reliability and evaluating the performance.

Based on the analysis in Section II-B, $\varphi^*_{k,m} = \angle h_{k,m} - \angle h_{ar,m}$ and $\tilde{\varphi}_{k,m} = \varphi^*_{k,m} + \bar{\varphi}_{k,m}$, so we have: $\tilde{\varphi}_{k,m} = \angle h_{k,m} - \angle h_{ar,m} + \bar{\varphi}_{k,m}$. Correspondingly, the cascaded channel $\mathbf{g}_k^H \tilde{\mathbf{\Theta}}_k \mathbf{h}_{ar}$ can be re-expressed as

$$\mathbf{h}_k^H \tilde{\mathbf{\Theta}}_k \mathbf{h}_{ar} = \sqrt{\beta_k} \bar{h}_k \bar{h}_{ar} \sum\nolimits_{m=1}^{M} |\tilde{h}_{k,m}||\tilde{h}_{ar,m}| e^{j\bar{\varphi}_{k.m}}. \tag{9}$$

Let $Z_k = \left|\sum_{m=1}^{M} |\tilde{h}_{k,m}||\tilde{h}_{ar,m}| e^{j\bar{\varphi}_{k.m}}\right|^2$ and $\varpi_k = P_s \beta_k \bar{h}_k^2 \bar{h}_{ar}^2 / \sigma_0^2$, with (7) and (8) , then the SINR for decoding common and private information can be respectively re-expressed as

$$\gamma_{c,k} = \frac{a_c \varpi_k Z_k}{(a_k + a_{\bar{k}}) \varpi_k Z_k + 1}, \tag{10}$$

$$\text{and} \quad \gamma_{p,k} = \frac{a_k \varpi_k Z_k}{a_{\bar{k}} \varpi_k Z_k + 1}. \tag{11}$$

According to the definition of OP, the communication outage event will occur when the rate of U_k is less than a predetermined target rate R_k^{th}. Based on this, let $\gamma_c^{th} = 2^{R_c^{th}} - 1$, $\gamma_k^{th} = 2^{R_k^{th}} - 1$, then the OP of U_k $(k \in \{t, r\})$ can be expressed as

$$OP_k = 1 - \Pr\left(\gamma_{c,k} > \gamma_c^{th}, \gamma_{p,k} > \gamma_k^{th}\right), \tag{12}$$

where the probability $\Pr(\gamma_{c,k} > \gamma_c^{th})$ can be given by

$$\begin{aligned} \Pr(\gamma_{c,k} > \gamma_c^{th}) &= \Pr\left(\tfrac{a_c \varpi_k Z_k}{(a_k + a_{\bar{k}}) \varpi_k Z_k + 1} > \gamma_c^{th}\right) \\ &= \Pr\left(Z_k > \tfrac{\gamma_c^{th}}{(a_c - (a_k + a_{\bar{k}}) \gamma_c^{th}) \varpi_k} = \tilde{\gamma}_{c,k}^{th}\right), \end{aligned} \tag{13}$$

and the probability $\Pr(\gamma_{_{p,k}} > \gamma_{_k}^{th})$ can be given by

$$\begin{aligned} \Pr(\gamma_{_{p,k}} > \gamma_{_k}^{th}) &= \Pr\left(\tfrac{a_k \varpi_k Z_k}{a_{\bar{k}} \varpi_k Z_k + 1} > \gamma_k^{th}\right) \\ &= \Pr\left(Z_{_k} > \tfrac{\gamma_{_k}^{th}}{a_{_k} \varpi_{_k} - a_{\bar{k}} \varpi_{_k} \gamma_{_k}^{th}} = \tilde{\gamma}_{p,k}^{th}\right), \end{aligned} \tag{14}$$

where $\tilde{\gamma}_{c,k}^{th} = \frac{\gamma_c^{th} \varpi_k^{-1}}{a_c - (a_k + a_{\bar{k}}) \gamma_c^{th}}$ and $\tilde{\gamma}_{p,k}^{th} = \frac{\gamma_k^{th} \varpi_k^{-1}}{a_k - a_{\bar{k}} \gamma_k^{th}}$. To ensure that the thresholds $\tilde{\gamma}_{c,k}^{th}$ and $\tilde{\gamma}_{p,k}^{th}$ are larger than zero, the PA coefficients need to satisfy the following constraints.

$$a_c > (a_k + a_{\bar{k}}) \gamma_c^{th}, \; a_k > a_{\bar{k}} \gamma_k^{th}. \tag{15}$$

Otherwise, the outage will occur. With (13) and (14), the OP given in (12) can be re-written as

$$\begin{aligned} OP_k &= 1 - \Pr\left(Z_k > \tilde{\gamma}_{c,k}^{th}, Z_k > \tilde{\gamma}_{p,k}^{th}\right) \\ &= 1 - \Pr\left(Z_k > \Upsilon_k\right) \\ &= \Pr\left(Z_k \le \Upsilon_k\right) = F_{Z_k}(\Upsilon_k), \end{aligned} \tag{16}$$

where $\Upsilon_k = \max\{\tilde{\gamma}_{c,k}^{th}, \tilde{\gamma}_{p,k}^{th}\}$ and $F_{Z_k}(x)$ is the cumulative distribution function (CDF) of Z_k. In what follows, we introduce the Lemma 1 to show the OP of user k.

Lemma 1. *For legitimate user k, its OP can be given by*

$$OP_k \simeq \frac{\tilde{\Gamma}\left(\mathcal{O}_k, \mathcal{C}_k \Upsilon_k\right)}{\Gamma\left(\mathcal{O}_k\right)} \quad, \; k \in \{t, r\}. \tag{17}$$

Proof: According to the definition of Z_k, it can be re-expressed as

$$Z_k = \left|\sum\nolimits_{m=1}^{M} |\tilde{h}_{k,m}||\tilde{h}_{ar,m}| e^{j\bar{\varphi}_{k,m}}\right|^2 = {T_k}^2 + {W_k}^2, \tag{18}$$

where $T_k = \sum_{m=1}^{M} |\tilde{h}_{k,m}||\tilde{h}_{ar,m}| \cos(\bar{\varphi}_{k,m})$ and $W_k = \sum_{m=1}^{M} |\tilde{h}_{k,m}||\tilde{h}_{ar,m}| \sin(\bar{\varphi}_{k,m})$.

Considering that the number of STAR-RIS elements, M is large in general, Z_k can be approximated as a Gamma random variable with the shape parameter $\mathcal{O}_k = \frac{\{\mathbb{E}(Z_k)\}^2}{\mathbb{D}(Z_k)}$ and rate parameter $\mathcal{C}_k = \frac{\mathbb{E}(Z_k)}{\mathbb{D}(Z_k)}$ [32]. Thus, we have: $Z_k \sim \Gamma(\mathcal{O}_k, \mathcal{C}_k)$. Based on this, the PDF of Z_k can be approximated as

$$f_{z_k}(z) \simeq \frac{(\mathcal{C}_k)^{\mathcal{O}_k}}{\Gamma(\mathcal{O}_k)} z^{\mathcal{O}_k - 1} e^{-\mathcal{C}_k z}, \tag{19}$$

where $\mathcal{O}_k$ and $\mathcal{C}_k$ can be respectively deduced as

$$\begin{aligned} &\mathcal{O}_k = \tfrac{(MV_{\Phi,k}(1+\lambda_k)+MV_{\Psi,k})^2}{2(MV_{\Phi,k})^2(1+2\lambda_k)+2(MV_{\Psi,k})^2}, \\ &\text{and } \mathcal{C}_k = \tfrac{MV_{\Phi,k}(1+\lambda_k)+MV_{\Psi,k}}{2(MV_{\Phi,k})^2(1+2\lambda_k)+2(MV_{\Psi,k})^2}, \end{aligned} \tag{20}$$

where $V_{\Psi,k} = \hat{h}_f^4 \left(\frac{\Gamma(\mu)\Gamma(\mu+2/\alpha)}{\Gamma^2(\mu+1/\alpha)}\right)^2 \left(\frac{1-\sin c(2\upsilon\pi)}{2}\right)$, $V_{\Phi,k} = \hat{h}_f^4 \left(\frac{\Gamma(\mu)\Gamma(\mu+2/\alpha)}{\Gamma^2(\mu+1/\alpha)}\right)^2 \left(\frac{1+\sin c(2\upsilon\pi)}{2}\right) - \hat{h}_f^4 \sin c^2(\upsilon\pi)$, and $\lambda_k = \frac{M\hat{h}_f^4 \sin c^2(\upsilon\pi)}{V_{\Phi,k}}$. The detailed derivation on (20) can refer to Appendix A.

With (19), the CDF of Z_k can be given by

$$F_{Z_k}(z) \simeq \frac{\tilde{\Gamma}(\mathcal{O}_k, \mathcal{C}_k z)}{\Gamma(\mathcal{O}_k)}, \tag{21}$$

where $\tilde{\Gamma}(a,x) = \int_0^x t^{a-1} e^{-t} dt$ [30]. Substituting (21) into (16) yields (17). ■

Equation (17) is an approximate closed-form expression of OP for U_k ($k \in \{t,r\}$), and it can match the simulation well, especially for large M. Thus, it can be used for the following performance evaluation and optimization.

For perfect phase design, the phase error $\bar{\varphi}_{k,m} = 0$ (i.e., $\upsilon \to 0$, which corresponds to $b \to +\infty$). Based on these results, with the derivation in Appendix A, using (71)-(73), we can obtain:

$$\begin{aligned} &\bar{\Phi}_k = \mathbb{E}(\Phi_{k,m}) = \Omega_k, \\ &V_{\Phi,k} = \mathbb{D}(\Phi_{k,m}) = (V_k + \Omega_k^2) - \Omega_k^2 = V_k, \\ &V_{\Psi,k} = \mathbb{D}(\Psi_{k,m}) = 0. \end{aligned} \tag{22}$$

Thus, the non-central parameter λ_k in (74) becomes

$$\lambda_k = M\hat{h}_f^4 / V_k. \tag{23}$$

Substituting (22) and (23) into (20) gives

$$\hat{\mathcal{O}}_k = \tfrac{(V_k + M\hat{h}_f^4)^2}{2(V_k + 2M\hat{h}_f^4)V_k}, \ \hat{\mathcal{C}}_k = \tfrac{V_k + M\hat{h}_f^4}{2MV_k(V_k + 2M\hat{h}_f^4)}. \tag{24}$$

Then, substituting (24) into (17) yields

$$OP_k \simeq \tilde{\Gamma}(\hat{\mathcal{O}}_k, \hat{\mathcal{C}}_k \Upsilon_k)/\Gamma(\hat{\mathcal{O}}_k). \tag{25}$$

Equation (25) is an approximate closed-form expression of OP for U_k ($k \in \{t,r\}$) under perfect phase design.

IV. Covert performance analysis

In this section, we will present the covert performance analysis of the STAR-RIS aided THz-RSMA system, derive the ADEP for the performance evaluation. Based on this, the optimal threshold is proposed to minimizes the ADEP.

A. Detection at the Warden

We consider a covert communication where the AP (Alice) sends the information x_c and x_t to public user Carl (U_t) continuously, also covert information x_r to the target user Bob (U_r) according to the previously scheduled time with Bob. The signals x_c and x_t, which are the public information, also act as artificial noise and play a covering role for the covert information x_r. Based on this, we propose two hypotheses as H_0 and H_1. The received signals at Willie for the two hypotheses can be expressed as

$$y_w[l] = \begin{cases} \mathbf{h}_w^H \tilde{\mathbf{\Theta}}_r \mathbf{h}_{ar} x_0[i] + n_w[i] & H_0 \\ \mathbf{h}_w^H \tilde{\mathbf{\Theta}}_r \mathbf{h}_{ar} x_1[i] + n_w[i] & H_1 \end{cases}, \tag{26}$$

where H_0 indicates that no covert information is sent and H_1 indicates that covert information is sent. $x_0 = \sqrt{a_c P_s} x_c[i] + \sqrt{a_t P_s} x_t[i]$, $n_w[i]$ is uncertain noise received at Willie with the distribution as $n_w[i] \sim \mathcal{CN}(0, \sigma_w^2)$. Considering the randomness of the noise power to interfere Willie's detection, the noise power obeys a uniform distribution over $[\eta^l, \eta^u]$ [33]. Correspondingly, the PDF is given by

$$f_{\sigma_w^2}(x) = \begin{cases} \dfrac{1}{\eta^u - \eta^l} & \eta^l \le x \le \eta^u \\ 0 & other \end{cases}. \tag{27}$$

In a covert communication system, the warden Willie needs to determine whether the Alice sends a covert message in terms of the received signal power T_w. Here, the Neyman-Pearson criterion [34] is used for judgment at Willie with a detection threshold of τ. Correspondingly, a radiometer is employed at Willie given by

$$P_w \underset{D_1}{\overset{D_0}{\lessgtr}} \tau, \tag{28}$$

where D_0 and D_1 are binary decisions corresponding to H_0 and H_1, respectively, by which Willie determines whether the AP has sent covert information. In this paper, we consider an infinitely long communication time slot (i.e. $I \to \infty$) [35], [36]. The average received power P_w at Willie is denoted as

$$P_w = \begin{cases} (a_c + a_t)|\mathbf{h}_w^H \tilde{\mathbf{\Theta}}_r \mathbf{h}_{ar}|^2 P_s + \sigma_w^2 & H_0 \\ |\mathbf{h}_w^H \tilde{\mathbf{\Theta}}_r \mathbf{h}_{ar}|^2 P_s + \sigma_w^2 & H_1. \end{cases} \tag{29}$$

The prior probabilities of hypotheses H_0 and H_1 are assumed to be equal. Thus, the detection performance of Willie is measured by the DEP, which is defined as [37] [38]

$$\xi = P_{FA} + P_{MD}, \tag{30}$$

where $P_{FA} = \Pr\{D_1|H_0\} = \Pr\{P_w > \tau|H_0\}$ is the false alarm (FA) probability, which means that the AP does not send covert information but Willie determines that covert information is sent. $P_{MD} = \Pr\{D_0|H_1\} = \Pr\{P_w < \tau|H_1\}$ is the missed detection (MD) probability, which indicates that the AP sends covert information but Willie's judgment is that no covert information is sent. When $\xi = 0$, it represents the case that Willie has not detected an error, and $\xi = 1$ shows that Willie has always detected an error. In practice, the communication system needs to satisfy $\xi \ge 1 - \varepsilon$ in order to meet certain covert requirements, where $\varepsilon > 0$ is small value in general and it depends on the covertness requirement.

B. Detection Error Probability

From (26), the cascaded channel of AP-STAR-RIS-U_r link can be attained as

$$\mathbf{h}_w^H \tilde{\mathbf{\Theta}}_r \mathbf{h}_{ar} = \sum_{m=1}^{M} |\tilde{h}_{w,m}||\tilde{h}_{ar,m}| e^{j\varphi_{w.m}}, \tag{31}$$

where the phase $\varphi_{w,m} = \varphi_{r,m}^* + \bar{\varphi}_{r,m} - \angle h_{w,m} + \angle h_{ar,m}$, $\varphi_{r,m}^*$ is the STAR-RIS phase corresponding to U_r and $\bar{\varphi}_{r,m}$ is the discrete phase error. Thus, we have: $\varphi_{w,m} = \angle h_{r,m} - \angle h_{ar,m} + \bar{\varphi}_{r,m} - \angle h_{w,m} + \angle h_{ar,m} = \angle h_{r,m} - \angle h_{w,m} + \bar{\varphi}_{r,m}$. Since the channel information of the legitimate users is unknown to Willie, such as $\mathbf{h}_r$, the phase $\varphi_{w,m}$ can follow a uniform distribution of $[0, 2\pi]$ [33].

Let $X_w = |\mathbf{h}_w^H \tilde{\mathbf{\Theta}}_r \mathbf{h}_{ar}|^2$, then with (31), we have:

$$X_w = \left| \sum_{m=1}^{M} |\tilde{h}_{w,m}||\tilde{h}_{ar,m}| e^{j\varphi_{w,m}} \right|^2. \tag{32}$$

Considering that M is large in general, X_w can be approximated as an exponential distribution with parameter θ_w according to the Central Limit Theorem (CLT). Correspondingly, the PDF of X_w is shown as Lemma 2.

Lemma 2. *It can be shown that the PDF of X_w in (32) is given by*

$$f_{X_w}(x) \simeq (1/\theta_w) e^{-x/\theta_w}, \tag{33}$$

where the parameter $\theta_w = M \frac{\Gamma^2(\mu)\Gamma^2(\mu+2/\alpha)}{\Gamma^4(\mu+1/\alpha)} \hat{h}_f^4$.

Proof: Please refer to Appendix B. ■

Using (33), the CDF of X_w can be attained as

$$\text{and } F_{X_w}(x) \simeq 1 - e^{-x/\theta_w}, \tag{34}$$

With (29), the average received power at Willie can be attained as

$$P_w = \begin{cases} (a_c + a_t) P_s \beta_r \overline{h}_w^2 \overline{h}_{ar}^2 X_w + \sigma_w^2 & H_0 \\ P_s \beta_r \overline{h}_w^2 \overline{h}_{ar}^2 X_w + \sigma_w^2 & H_1 \end{cases}. \tag{35}$$

Based on the definitions of FA probability and MD probability in section IV-A, using (27) and (34), the FA probability and MD probability can be respectively derived as

$$\begin{aligned} P_{FA} &= \Pr\left\{ (a_c + a_t) P_s \beta_r \bar{h}_w^2 \bar{h}_{ar}^2 X_w + \sigma_w^2 > \tau \right\} \\ &= \begin{cases} 1 & \tau < \eta^l \\ \frac{\eta^u - \tau}{\eta^u - \eta^l} + \frac{v_1}{\eta^u - \eta^l} \left(1 - e^{\frac{\eta^l - \tau}{v_1}} \right) & \eta^l \le \tau \le \eta^u \\ \frac{v_1}{\eta^u - \eta^l} \left(e^{\frac{\eta^u}{v_1}} - e^{\frac{\eta^l}{\nu_1}} \right) e^{\frac{-\tau}{v_1}} & \tau > \eta^u \end{cases}, \end{aligned} \tag{36}$$

and

$$\begin{aligned} P_{MD} &= \Pr\left\{ P_s \beta_r \bar{h}_w^2 \bar{h}_{ar}^2 X_w + \sigma_w^2 < \tau \right\} \\ &= \begin{cases} 0 & \tau < \eta^l \\ \frac{\tau - \eta^l}{\eta^u - \eta^l} - \frac{v_2}{\eta^u - \eta^l} \left(1 - e^{\frac{\eta^l - \tau}{v_2}} \right) & \eta^l \le \tau \le \eta^u \\ 1 - \frac{v_2}{\eta^u - \eta^l} \left(e^{\frac{\eta^u}{v_2}} - e^{\frac{\eta^l}{v_2}} \right) e^{\frac{-\tau}{v_2}} & \tau > \eta^u \end{cases}, \end{aligned} \tag{37}$$

where $v_1 = (a_c + a_t) \beta_r \bar{h}_w^2 \bar{h}_{ar}^2 P_s \theta_w$, $v_2 = \beta_r \bar{h}_w^2 \bar{h}_{ar}^2 P_s \theta_w$. Considering that $a_c + a_t = 1 - a_r < 1$, we have: $v_1 < v_2$. Correspondingly, $(\eta^l - \eta^u)/v_1 < (\eta^l - \eta^u)/v_2$ since $\eta^l < \eta^u$. Based on this, we can obtain:

$$\ln(1 - e^{\frac{\eta^l - \eta^u}{v_1}}) > \ln(1 - e^{\frac{\eta^l - \eta^u}{v_2}}). \tag{38}$$

Substituting (36) and (37) into (30) gives the expression of ADEP as (39), which is shown at the top of next page.

C. Optimal Detection Threshold

In this subsection, the optimal detection threshold is derived to minimize the ADEP (i.e., ξ in (39)). For Willie, to achieve the superior detection performance, the optimal threshold τ^* needs to be designed such that ξ can be minimized. Based on Eq.(39), it can be shown that $\xi \leqslant 1$. Moreover, when $\tau \le \eta^l$, ξ=1, so the optimal τ should exist in $(\eta^l, +\infty)$ to obtain the minimal ξ.

For convenient analysis, we define the function $\psi(\tau) = \xi$. Hence, in terms of (39), when $\eta^l < \tau \le \eta^u$, we can calculate the partial derivative of the ψ with respect to (w.r.t.) τ as

$$\frac{\partial \psi(\tau)}{\partial \tau} = \frac{1}{\eta^u - \eta^l} \left(e^{\frac{\eta^l - \tau}{v_1}} - e^{\frac{\eta^l - \tau}{v_2}} \right) < 0, \tag{40}$$

where $v_1 < v_2$ and $\tau > \eta^l$ are utilized. Hence, $\psi(\tau)$ is a decreasing function w.r.t. τ for $\tau \in (\eta^l, \eta^u]$. Thus, when $\tau = \eta^u$, the minimal ξ, ξ^* is attained, i.e.,

$$\begin{aligned} \xi^* = \psi(\eta^u) = 1 + \frac{v_1}{\eta^u - \eta^l} (1 - e^{\frac{\eta^l - \eta^u}{v_1}}) \\ - \frac{v_2}{\eta^u - \eta^l} (1 - e^{\frac{\eta^l - \eta^u}{v_2}}), \;\; \eta^l < \tau \le \eta^u. \end{aligned} \tag{41}$$

When $\tau \ge \eta^u$, we can calculate the partial derivative of the ψ w.r.t. τ as

$$\begin{aligned} \frac{\partial \psi(\tau)}{\partial \tau} &= \frac{1}{\eta^u - \eta^l} \left[(e^{\frac{\eta^u}{v_2}} - e^{\frac{\eta^l}{v_2}}) e^{\frac{-\tau}{v_2}} - (e^{\frac{\eta^u}{v_1}} - e^{\frac{\eta^l}{v_1}}) e^{\frac{-\tau}{v_1}} \right] \\ &= \frac{1}{\eta^u - \eta^l} (A e^{\frac{-\tau}{v_2}} - B e^{\frac{-\tau}{v_1}}), \end{aligned} \tag{42}$$

where $A = e^{\frac{\eta^u}{v_2}} - e^{\frac{\eta^l}{v_2}} > 0$ and $B = e^{\frac{\eta^u}{v_1}} - e^{\frac{\eta^l}{v_1}} > 0$. By setting $\frac{\partial \psi(\tau)}{\partial \tau} = 0$, we can obtain the threshold value as

$$\tau^o = \frac{v_1 v_2 (\ln B - \ln A)}{v_2 - v_1} = \frac{\ln B - \ln A}{v_1^{-1} - v_2^{-1}}. \tag{43}$$

Firstly, we present the Theorem 1 to show the $\tau^o > \eta^u$.

Theorem 1. *For τ^o in (43), it is shown that $\tau^o > \eta^u$.*

Proof: According to the definition of the parameters A and B, we have:

$$\begin{aligned} &\ln B - \ln A \\ &= \ln \left(e^{\frac{\eta^u}{v_1}} (1 - e^{\frac{\eta^l - \eta^u}{v_1}}) \right) - \ln \left(e^{\frac{\eta^u}{v_2}} (1 - e^{\frac{\eta^l - \eta^u}{v_2}}) \right) \\ &= \frac{\eta^u}{v_1} - \frac{\eta^u}{v_2} + \ln \left(1 - e^{\frac{\eta^l - \eta^u}{v_1}} \right) - \ln \left(1 - e^{\frac{\eta^l - \eta^u}{v_2}} \right). \end{aligned} \tag{44}$$

Substituting (38) into (44) yields

$$\ln B - \ln A > \frac{\eta^u}{v_1} - \frac{\eta^u}{v_2} = \eta^u (v_1^{-1} - v_2^{-1}). \tag{45}$$

$$\xi=\begin{cases}1 & \tau\le\eta^{l}\\ 1+\frac{v_1}{\eta^u-\eta^l}\left(1-e^{\frac{\eta^l-\tau}{v_1}}\right)-\frac{v_2}{\eta^u-\eta^l}\left(1-e^{\frac{\eta^l-\tau}{v_2}}\right) & \eta^l<\tau\le\eta^u\\ 1+\frac{v_1}{\eta^u-\eta^l}\left(e^{\frac{\eta^u}{v_1}}-e^{\frac{\eta^l}{v_1}}\right)e^{\frac{-\tau}{v_1}}-\frac{v_2}{\eta^u-\eta^l}\left(e^{\frac{\eta^u}{v_2}}-e^{\frac{\eta^l}{v_2}}\right)e^{\frac{-\tau}{v_2}} & \tau>\eta^u\end{cases}. \tag{39}$$

Since $v_1^{-1}>v_2^{-1}$, with (45), we can obtain:

$$\tau^o=\frac{\ln B-\ln A}{v_1^{-1}-v_2^{-1}}>\eta^u. \tag{46}$$

■

Then, the Lemma 3 is introduced to show the τ^o is optimal detection threshold.

Lemma 3. *For the ADEP in (39), there exists an optimal detection threshold τ^o in (43) that can minimize the ADEP ξ.*

Proof: Since $\eta^u<\tau^o$, when $\eta^u\le\tau<\tau^o$, we have: $\frac{\partial\psi(\tau)}{\partial\tau}<0$. In the following, we give the corresponding proof. When $\tau<\tau^o$, with (43), we can obtain that $\frac{\ln B-\ln A}{v_1^{-1}-v_2^{-1}}>\tau$. Since $v_1^{-1}>v_2^{-1}$, we have:

$$\ln(B/A)>\tau/v_1-\tau/v_2. \tag{47}$$

Thus, $B/A>e^{\tau/v_1}e^{-\tau/v_2}$. Because $A>0$ and $e^{\tau/v_1}>0$, with (47), we can obtain:

$$Be^{-\tau/v_1}>Ae^{-\tau/v_2}. \tag{48}$$

Substituting (51) into (42) yields $\frac{\partial\psi(\tau)}{\partial\tau}<0$. Similarly, we can prove that $\frac{\partial\psi(\tau)}{\partial\tau}>0$ when $\tau>\tau^o$.

According to the analysis above, when $\eta^u\le\tau\le\tau^o$, $\psi(\tau)$ is a decreasing function w.r.t. τ, while when $\tau\ge\tau^o$, $\psi(\tau)$ is an increasing function w.r.t. τ. Hence, for $\tau\ge\eta_u$, ξ can take the minimal value ξ^* when $\tau=\tau^o$. Moreover, $\psi(\tau^0)<\psi(\eta_u)$ due to the decreasing function of $\psi(\tau)$ for $\tau\in[\eta^u,\tau^o]$. Furthermore, considering that $\psi(\tau)$ is a decreasing function w.r.t. τ for $\tau\in(\eta^l,\eta^u]$, ξ^*= $\psi(\tau^o)$ is also minimal for $\tau>\eta^l$. Hence, there exists an optimal detection threshold τ^o, and when $\tau=\tau^o$, the minimal ξ is attained. ■

Based on the above results, we present the Theorem 2 for the minimal ADEP ξ^* as follows.

Theorem 2. *The minimal ADEP, ξ^* can be given by (49), and it is a decreasing function on the transmit power P_s.*

$$\xi^*=1+\frac{v_1-v_2}{\eta^u-\eta^l}B\left(\frac{A}{B}\right)^{1/a_r}. \tag{49}$$

Proof: Based on the optimal threshold τ^o, we substitute (46) into (39), and resultant minimal ADEP is given by

$$\begin{aligned}\xi^*=1&+\frac{v_1}{\eta^u-\eta^l}\left(e^{\frac{\eta^u}{v_1}}-e^{\frac{\eta^l}{v_1}}\right)e^{\frac{-\tau^o}{v_1}}\\ &-\frac{v_2}{\eta^u-\eta^l}\left(e^{\frac{\eta^u}{v_2}}-e^{\frac{\eta^l}{v_2}}\right)e^{\frac{-\tau^o}{v_2}}.\end{aligned} \tag{50}$$

Substituting $A=e^{\frac{\eta^u}{v_2}}-e^{\frac{\eta^l}{v_2}}>0$ and $B=e^{\frac{\eta^u}{v_1}}-e^{\frac{\eta^l}{v_1}}>0$ into (50) yields

$$\begin{aligned}\xi^*&=1+\frac{v_1}{\eta^u-\eta^l}Be^{\frac{\ln(A/B)}{a_r}}\\ &\quad-\frac{v_2}{\eta^u-\eta^l}Ae^{\frac{(1-a_r)}{a_r}\ln(A/B)}\\ &=1+\frac{v_1}{\eta^u-\eta^l}B\left(\frac{A}{B}\right)^{1/a_r}-\frac{v_2}{\eta^u-\eta^l}A\left(\frac{A}{B}\right)^{1/a_r}\frac{B}{A}\\ &=1+\frac{v_1-v_2}{\eta^u-\eta^l}B\left(\frac{A}{B}\right)^{1/a_r}.\end{aligned} \tag{51}$$

Thus, (49) is attained. With (51), we can calculate the $\partial\xi^*/\partial P_s$ as

$$\frac{\partial\xi^*}{\partial P_s}=-\frac{a_r}{\eta^u-\eta^l}\left(\frac{A}{B}\right)^{1/a_r}\beta_r\bar{h}_w^2\bar{h}_{ar}^2\theta_wB<0. \tag{52}$$

Hence, the ADEP ξ^* is a decreasing function on the transmit power P_s.

■

Furthermore, for a fixed power P_s, we present the Theorem 3 to show that the minimal ADEP is a decreasing function on the PA coefficient a_r.

Theorem 3. *The minimal ADEP, ξ^* is a decreasing function on the PA coefficient a_r for the fixed power P_s.*

Proof: Let $t=1/a_r$, then we have:

$$\begin{aligned}&\xi^*=1-v_2A^tB^{(1-t)}/[(\eta^u-\eta^l)t]\\ &\text{and } \frac{\partial B}{\partial t}=-\frac{1}{(t-1)^2v_2}[\eta^ue^{\frac{t\eta^u}{(t-1)v_2}}-\eta^le^{\frac{t\eta^l}{(t-1)v_2}}],\end{aligned} \tag{53}$$

where $B=e^{\frac{\eta^u}{v_1}}-e^{\frac{\eta^l}{v_1}}=e^{\frac{t\eta^u}{(t-1)v_2}}-e^{\frac{t\eta^l}{(t-1)v_2}}$. Using (53), we can calculate $\partial\xi^*/\partial t$ as

$$\begin{aligned}\frac{\partial\xi^*}{\partial t}&=\frac{A^tB^{(1-t)}}{t}[\frac{1}{t}+\ln(\frac{B}{A})\\ &\quad+\frac{1}{(1-t)v_2B}(\eta^ue^{\frac{t\eta^u}{(t-1)v_2}}-\eta^le^{\frac{t\eta^l}{(t-1)v_2}})]\\ &>\frac{A^tB^{1-t}}{t}[\frac{1}{t}+\ln(\frac{B}{A})+\frac{B^{-1}}{(1-t)v_2}(\eta^le^{\frac{t\eta^u}{(t-1)v_2}}-\eta^le^{\frac{t\eta^l}{(t-1)v_2}})]\\ &=\frac{A^tB^{1-t}}{t}[\frac{1}{t}+\ln(\frac{B}{A})+\frac{\eta^l}{(1-t)v_2}]>0,\end{aligned} \tag{54}$$

where $A,B,t,v_2,(1-t),\eta_l>0$, and $B>A$ are all utilized. Hence, with $t=1/a_r$, we can obtain that $\frac{\partial\xi^*}{\partial a_r}=-\frac{\partial\xi^*}{\partial t}\frac{1}{a_r^2}<0$. Thus, the ξ^* is a decreasing function on a_r. ■

According to the results above, when a_r arrives at its maximum value, the ξ^* can obtain its minimum value. Based on this, when a_r tends to be 1, the minimal ξ^* is given by

$$\begin{aligned}\tilde{\xi}^*&=\lim_{a_r\to1}\xi^*=\lim_{a_r\to1}1-\frac{a_rv_2}{\eta^u-\eta^l}A^{\frac{1}{a_r}}B^{1-\frac{1}{a_r}}\\ &=1-\frac{v_2A}{\eta^u-\eta^l}e^{-\frac{\eta^u}{v_2}}.\end{aligned} \tag{55}$$

Normally, the $\tilde{\xi}^*$ is not equal to zero, but when the power P_s tends to be infinite, the $\tilde{\xi}^*$ will be zero. Specifically, let $c=1/v_2$, then $c\to0$ since $v_2,P_s\to+\infty$. Thus, we have:

$$\lim_{P_s\to+\infty}\tilde{\xi}^*=\lim_{c\to0}1-\frac{e^{\eta^uc}-e^{\eta^lc}}{(\eta^u-\eta^l)c}=1-\frac{\eta^u-\eta^l}{\eta^u-\eta^l}=0. \tag{56}$$

In what follows, we introduce the Lemma 4 to show the asymptotical property of the ADEP in (49) under large power.

Lemma 4. *When transmit power P_s is very large, the ADEP in (49), ξ^* will tend to be $1-a_r(1-a_r)^{(1/a_r-1)}$, and is also a decreasing function of a_r.*

Proof: When P_s is very large, substituting $A=e^{\frac{\eta^u}{v_2}}-e^{\frac{\eta^l}{v_2}}$ and $B=e^{\frac{\eta^u}{v_1}}-e^{\frac{\eta^l}{v_1}}$ into (49), we can deduce that

$$\lim_{P_s\to+\infty}\frac{A}{B}=\lim_{P_s\to+\infty}\left(e^{\frac{\eta^l}{v_2}-\frac{\eta^l}{v_1}}\right)\frac{e^{\frac{\eta^u-\eta^l}{v_2}}-1}{e^{\frac{\eta^u-\eta^l}{v_1}}-1}=(1-a_r),$$
$$\text{and}\lim_{P_s\to+\infty}\frac{(v_1-v_2)B}{\eta^u-\eta^l}=\lim_{P_s\to+\infty}\frac{v_1-v_2}{\eta^u-\eta^l}\left(e^{\frac{\eta^u}{v_1}}-e^{\frac{\eta^l}{v_1}}\right)=\frac{a_r}{a_r-1}, \tag{57}$$

where $v_2=\beta_r\bar{h}_w^2\bar{h}_{ar}^2P_s\theta_w$, and $v_1=(1-a_r)v_2$ are utilized.

Hence, using (57) and (49), the asymptotic ADEP at high power can be derived as

$$\hat{\xi}^*=\lim_{P_s\to+\infty}\xi^*=1-a_r(1-a_r)^{(1/a_r-1)}. \tag{58}$$

Using (58), considering $a_r\in(0,1)$, we can calculate the $\partial\hat{\xi}^*/\partial a_r$ as

$$\frac{\partial\hat{\xi}^*}{\partial a_r}=(1-a_r)^{(1/a_r-1)}\frac{1}{a_r}\ln(1-a_r)<0. \tag{59}$$

Thus, $\hat{\xi}^*$ is a decreasing function on a_r. Besides, with (58), we can obtain

$$\lim_{a_r\to1}\hat{\xi}^*=\lim_{a_r\to1}1-a_r(1-a_r)^{(1/a_r-1)}=0, \tag{60}$$

which is also consistent with (56). ■

From the Lemma above, it is interestingly found that the asymptotic ADEP at high power is only related to the PA coefficient of covert user a_r, and is a decreasing function on a_r, which can accord with the Theorem 3 as well. Hence, we can improve the covert performance by decreasing a_r for high power, and the $\hat{\xi}^*$ will be zero when a_r tends to be 1. Besides, since the ADEP ξ^* is a decreasing function on the power P_s, we have: $\xi^*\geq\hat{\xi}^*$.

V. PA SCHEME FOR OP MINIMIZATION

In this section, we will derive an adaptive PA scheme to minimize the OP of legitimate user Bob while meeting the constraints of reliability and covertness, where the PA coefficients a_c, a_r and a_t are jointly optimized. Correspondingly, the optimization problem is formulated as

$$\begin{aligned}&\min_{\{a_c,a_t,a_r\}}J=OP_r\\&\quad\text{s.t. }C_1:OP_t\leq\delta\\&\qquad\quad C_2:\xi^*\geq1-\varepsilon\\&\qquad\quad C_3:a_t+a_r+a_c=1\end{aligned} \tag{61}$$

where the δ is the predefined outage constraint of legitimate user Carl U_t, ε is the predefined limitation on the covertness performance of the system

The above problem is non-convex and difficult to be directly tackled. We can use the three-dimensional search method to solve the this problem, and resultant optimal PA coefficients can be attained. However, the complexity will become huge and increase exponentially with the number of optimized variables. Considering the C_3 constraint, the a_t can be obtained by $1-a_r-a_c$. Based on this, two-dimensional (2D) search method can be used to find the minimum OP_r by searching a_c over the interval $(0,1)$ and a_r over the interval $(0,1-a_c)$ while satisfying the constraints C_1 and C_2 as well as the constrains from (15). Considering that the ADEP is only related to the PA coefficient a_r, the search of a_r is placed in the outer loop, and the search of a_c is placed in the inner loop. Thus, the run efficiency is increased. Otherwise, the ADEP needs to be calculated by both outer loop and inner loop, which will brings poor efficiency. Specifically, the PA optimization algorithm procedure is summarized as Algorithm 1.

Algorithm 1 PA optimization algorithm for OP minimization based on 2D search method

Input: error tolerance ς;
Initialize: search interval: $ar_{in}=(0:\Delta_1:1)$, search step $\Delta_1>0$ is set in terms of ς;
Calculate the length of ar_{in} as L_1,
for $k=1:L_1$ **do**
  $a_r=ar_{in}(k)$,
  Calculate $a_c^u=1-a_r$;
  Set the search interval: $ac_{in}=(0:\Delta_2:a_c^u)$, search step $\Delta_2>0$ is set in terms of ς;
  Calculate the length of ac_{in} as L_2
  for $l=1:L_2$ **do**
    $a_c=ac_{in}(l)$,
    Calculate $a_t=1-a_r-a_c$;
    if $a_c>\frac{\gamma_c^{th}}{1+\gamma_c^{th}}$ and $a_r>a_t\gamma_r^{th}$ and $a_t>a_r\gamma_t^{th}$ **then**
      Calculate OP_t and OP_r by (17), and ξ^* by (49);
      if $OP_t\leq\delta$ and $\xi^*\geq1-\varepsilon$ **then**
        $J(k,l)=OP_r$;
      else
        $J(k,l)=1$;
      end if
    else
      $J(k,l)=1$;
    end if
  end for
end for
Calculate $(k^*,l^*)=\arg\min_{(k,l)}J(k,l)$;
Output: $a_r^*=ar_{in}(k^*)$, $a_c^*=ac_{in}(l^*)$, and $a_t^*=1-a_r^*-a_c^*$.

By performing the above algorithm, the optimal PA coefficients can be attained. According to the analysis above, however, the optimal scheme still has relatively high complexity because the 2D search method is employed, especially when search step is very small for achieving high precision. Based on this, we will propose a suboptimal PA scheme with low complexity in terms of 1D search method by analyzing the OP expression of legitimate user Bob and the OP constraint of legitimate user Carl. Correspondingly, the Lemma 5 is introduced for the scheme design.

Lemma 5. *It can be shown that the OP_r is a decreasing function with respect to a_c given the a_r.*

Proof: From (16), it can be shown that $F_{Z_k}(z)$ is an increasing function of z since the PDF of Z_k is positive. Hence, following (61), minimizing the OP of U_r, OP_r is equivalent to minimizing the parameter Υ_r in (16). Since Υ_r=$\max\{\tilde{\gamma}_{c,r}^{th}, \tilde{\gamma}_{p,r}^{th}\}$, we will consider two cases for achieving the minimum Υ_r.

Firstly, when $\tilde{\gamma}_{c,r}^{th} \leq \tilde{\gamma}_{p,r}^{th}$, $\Upsilon_r = \tilde{\gamma}_{p,r}^{th}$. Under this case, minimizing Υ_r is changed into minimizing $\tilde{\gamma}_{p,r}^{th}$. From the definition $\tilde{\gamma}_{p,r}^{th} = \frac{\gamma_r^{th}\varpi_r^{-1}}{a_r - a_t\gamma_r^{th}} = \frac{\gamma_r^{th}\varpi_r^{-1}}{a_c\gamma_r^{th} + a_r(1+\gamma_r^{th}) - \gamma_r^{th}}$, we can conclude that given a_r, the larger a_c is, the smaller $\tilde{\gamma}_{p,r}^{th}$ is.

Secondly, when $\tilde{\gamma}_{c,r}^{th} \geq \tilde{\gamma}_{p,r}^{th}$, $\Upsilon_r = \tilde{\gamma}_{c,r}^{th}$. Under this case, minimizing Υ_r is changed into minimizing $\tilde{\gamma}_{c,r}^{th}$. From the definition $\tilde{\gamma}_{c,r}^{th} = \frac{\gamma_c^{th}\varpi_r^{-1}}{a_c - (a_r+a_t)\gamma_c^{th}} = \frac{\gamma_c^{th}\varpi_r^{-1}}{a_c(1+\gamma_c^{th}) - \gamma_c^{th}}$, we can conclude that the larger a_c is, the smaller $\tilde{\gamma}_{c,r}^{th}$ is. Therefore, OP_r is a decreasing function of a_c given the a_r. ■

According to the above analysis, to minimize the OP_r, the a_c needs to be maximized given the a_r. With the OP_t and constraint C_1, a maximum a_c can be attained. Specifically, with the constraint C_1, considering that $F_{Z_t}(\Upsilon_t)$ in (16) is an increasing function of Υ_t, the following inequality can be derived as

$$\Upsilon_t = \max\{\tilde{\gamma}_{c,t}^{th}, \tilde{\gamma}_{p,t}^{th}\} \leq F_{Z_t}^{-1}(\delta) = \Xi_t, \tag{62}$$

where $\Xi_t = F_{Z_t}^{-1}(\delta)$ is a inverse function of $F_{Z_t}(z)$, and it can be calculated by the inverse of the regularized lower incomplete gamma function of Matlab software in terms of (17). Hence, with (62), when $\gamma_{c,t}^{th} \geq \tilde{\gamma}_{p,t}^{th}$, i.e., $a_c \leq a_c^{u1}$, where a_c^{u1} is an upper bound of a_c under this case and shown as follows:

$$a_c^{u1} = \frac{\gamma_c^{th}(1+\gamma_t^{th})(1-a_r)}{\gamma_t^{th} + \gamma_c^{th}(1+\gamma_t^{th})}, \tag{63}$$

we can obtain that $\tilde{\gamma}_{c,t}^{th} = \frac{\gamma_c^{th}\varpi_t^{-1}}{a_c - (a_r+a_t)\gamma_c^{th}} = \frac{\gamma_c^{th}\varpi_t^{-1}}{a_c(1+\gamma_c^{th}) - \gamma_c^{th}} \leq \Xi_t$. Thus, a lower bound of a_c under this case is give by

$$a_c^{l1} = \frac{\gamma_c^{th}(1+1/(\varpi_t\Xi_t))}{1+\gamma_c^{th}}. \tag{64}$$

When $\gamma_{p,t}^{th} > \tilde{\gamma}_{c,t}^{th}$, that is, $a_c > a_c^{u1}$, we can obtain that $\tilde{\gamma}_{p,t}^{th} = \frac{\gamma_t^{th}\varpi_t^{-1}}{a_t - a_r\gamma_t^{th}} = \frac{\gamma_t^{th}\varpi_t^{-1}}{1 - a_c - a_r - a_r\gamma_t^{th}} \leq \Xi_t$. Thus, another upper bound of a_c under this case can be attained as

$$a_c^{u2} = 1 - \gamma_t^{th}\varpi_t^{-1}\Xi_t^{-1} - (1+\gamma_t^{th})a_r. \tag{65}$$

With the analysis above, for the case of $\gamma_{p,t}^{th} > \tilde{\gamma}_{c,t}^{th}$, when $a_c^{u2} \geq a_c^{u1}$, we can obtain the maximum value of a_c, i.e., a_c^{u2}. However, when $a_c^{u2} < a_c^{u1}$, the case of $\gamma_{p,t}^{th} > \tilde{\gamma}_{c,t}^{th}$ will no longer hold since the C_1 does not meet. The Lemma 6 is introduced to show that $a_c^{u1} < a_c^{l1}$ under this case.

Lemma 6. *It can be shown that $a_c^{u1} < a_c^{l1}$ when $a_c^{u2} < a_c^{u1}$.*

Proof: From (65) and (63), when $a_c^{u2} < a_c^{u1}$, we can obtain:

$$1 - \frac{\gamma_t^{th}}{\varpi_t\Xi_t} - (1+\gamma_t^{th})a_r < \frac{\gamma_c^{th}(1+\gamma_t^{th})(1-a_r)}{\gamma_t^{th} + \gamma_c^{th}(1+\gamma_t^{th})}. \tag{66}$$

With (66), we have:

$$1 - a_r < \frac{[\gamma_t^{th} + \gamma_c^{th}(1+\gamma_t^{th})](1+1/(\varpi_t\Xi_t))}{(1+\gamma_t^{th})(1+\gamma_c^{th})}. \tag{67}$$

Thus, using (66), the following inequality can hold.

$$\begin{aligned} a_c^{u1} = \frac{\gamma_c^{th}(1+\gamma_t^{th})(1-a_r)}{\gamma_t^{th} + \gamma_c^{th}(1+\gamma_t^{th})} &< \frac{\gamma_c^{th}(1+\gamma_t^{th})(1+1/(\varpi_t\Xi_t))}{(1+\gamma_t^{th})(1+\gamma_c^{th})} \\ &= \frac{\gamma_c^{th}(1+1/(\varpi_t\Xi_t))}{1+\gamma_c^{th}} = a_c^{l1}. \end{aligned} \tag{68}$$

Hence, when $a_c^{u2} < a_c^{u1}$, $a_c^{u1} < a_c^{l1}$ is proved. ■

Therefore, when $a_c^{u2} < a_c^{u1}$, for $\gamma_{p,t}^{th} > \tilde{\gamma}_{c,t}^{th}$, the constraint C_1 can not be met, and for $\gamma_{p,t}^{th} \leq \tilde{\gamma}_{c,t}^{th}$, the constraint C_1 can not be met as well because $a_c^{u1} < a_c^{l1}$ under this case. Thus, the C_1 can be satisfied only when $a_c^{u2} \geq a_c^{u1}$. Under this case, we can achieve the maximum value of a_c, i.e., a_c^{u2} in (65). Based on this, the Υ_t and corresponding OP_r can be minimized. Moreover, when $a_c = a_c^{u2}$, with (65), we have: $a_c < 1 - (1+\gamma_t^{th})a_r$. Hence, $a_t > \gamma_t^{th}a_r$ in (15) can be met. Besides, considering $a_c > \frac{\gamma_c^{th}}{1+\gamma_c^{th}}$ in (15) and $a_c < 1 - a_r$, we can obtain that $a_r < 1/(1+\gamma_c^{th}) = a_r^u$. Thus, the search rang of a_r will become $(0, a_r^u)$, and corresponding range is reduced.

In terms of the above analysis, a suboptimal scheme based on the 1D search method is proposed to find the minimum OP_r by searching the a_r over the range $(0, a_r^u)$, while satisfying the constraints C_2 and $a_c^{u2} \geq a_c^{u1}$ as well as $a_t < a_r/\gamma_r^{th}$. Once the minimum OP_r while meeting the constraints is found, the a_r^* is attained. Correspondingly, the algorithm procedure is summarized as Algorithm 2 with 1D search.

Algorithm 2 PA optimization algorithm for OP minimization based on 1D search method

Input: error tolerance ς
Initialize: search interval: $ar_{in} = (0 : \Delta_a : a_r^u)$, search step $\Delta_a > 0$, which can be set in terms of ς.
Calculate the length of ar_{in} as L_a;
for $n = 1 : L_a$ **do**
  $a_r = ar_{in}(n)$,
  Calculate a_c^{u1} by (63) and a_c^{u2} by (65);
  Calculate ξ^* by (49);
  if $\xi^* \geq 1 - \varepsilon$ and $a_c^{u2} \geq a_c^{u1}$ **then**
    Calculate $a_c = a_c^{u2}$ and $\tilde{a}_c(n) = a_c$;
    Calculate $a_t = 1 - a_r - a_c$;
    if $a_r > a_t\gamma_r^{th}$ **then**
      Calculate OP_r by (17);
      $J(n) = OP_r$;
    else
      $J(n) = 1$;
    end if
  else
    $J(n) = 1$;
  end if
end for
Calculate $n^* = \arg\min_n J(n)$;
Output: $a_r^* = ar_{in}(n^*)$, $a_c^* = \tilde{a}_c(n^*)$, and $a_t^* = 1 - a_r^* - a_c^*$.

Regarding Algorithm 1, the main complexity involves 2D search, and thus it is approximated as $\mathcal{O}(1/\varsigma^2)$, where ς is the error tolerance. While for Algorithm 2, the main complexity is from 1D search, and it is approximated as $\mathcal{O}(1/\varsigma)$. Hence, the

Algorithm 2 has lower complexity than the Algorithm 1 due to its higher search efficiency, which can also be seen from the run time in simulation.

VI. Simulation results

In this section, the simulation results are provided to illustrate the accuracy of the presented theoretical analysis and the effectiveness of the proposed detection threshold and PA schemes. Also, the effect of different parameters on the covert performance of the systems is evaluated. Unless otherwise specified, main parameters are listed in Table I. Other parameters are set as: frequency $f = 300\text{GHz}$, $\kappa_{\tilde{\alpha}}(f) = 0.0033\text{m}^{-1}$ [40], $\eta^l = -85\text{dBm}$, and $\eta^u = -75\text{dBm}$ [41]. Simulation results are shown in Figs. 2-9, respectively.

TABLE I
Simulation parameters

Parameters	Default Values
Number of STAR-RIS elements	$M = 32$
Antenna gains	$G_t = 25\text{dBi}$, $G_r = 20\text{dBi}$
Rate thresholds	R_c^{th}=R_t^{th}=R_r^{th} = 0.5bit/s/Hz
Channel fading parameters	$\alpha = 2.5, \mu = 2$
Noise power	$\sigma_0^2 = -80\text{dBm}$
Distances	d_{ar}=5m, d_t=d_w=20m, d_r=15m
Equalization bit number	$b = 2$
PA coefficients	a_c= 0.6, a_t= 0.2, a_r= 0.2
Outage constraint of user Carl	$\delta = 0.1$
Covertness performance limitation	$\varepsilon = 0.1$

Fig. 2 and Fig. 3 respectively illustrate the outage probabilities of Bob (U_r) and Carl (U_t) under different numbers of STAR-RIS elements *M* and quantization bits *b*, where M=32, 64, b=2, 3, $+\infty$, theoretical OP is calculated by (17). From Fig.2 and Fig. 3, it can be seen that the theoretical OP matches the corresponding simulation well, which indicates that the presented outage analysis is valid. As the M increases, the outage performances of U_r and U_t are effectively improved, and corresponding OPs become lower. This is because larger number of STAR-RIS elements are used, which brings higher performance gain. Moreover, with the increase of b, the outage performance is improved as well since the phase errors become smaller. Especially under the ideal quantization condition ($b = +\infty$), the outage performances of users are better than those under the quantization error condition ($b = 2, 3$) for the same M. Namely, the users without quantization errors have lower OP than those with quantization errors, as expected. By comparison, it is found that increasing the number of elements of STAR-RIS is more effective. Thus, to maintain the same OP, we can increase the value of *M*, and resultant smaller transmit power is required.

Fig. 4 shows the outage performances of the users with different operating protocols of STAR-RIS, where the mode switching (MS) protocol [42] and our used energy splitting (ES) protocol for STAR-RIS are compared. For the sake of fairness, the number of STAR-RIS elements serving different users in MS protocol is $M/2$. As illustrate in Fig. 4, the OP of users with ES protocol is lower than that with MS protocol. This is because only subsets of the RIS elements are selected for transmission and reflection in the MS protocol, that is,

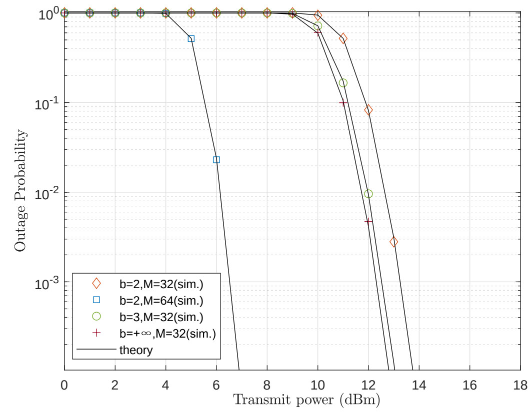

Fig. 2. OP of user U_r versus transmit power for different values of M and b.

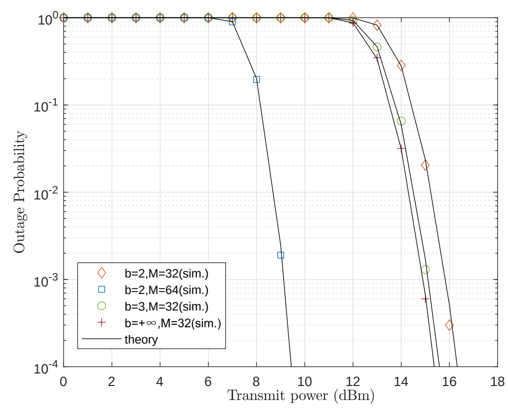

Fig. 3. OP of user U_t versus transmit power for different values of M and b.

the RIS elements in MS protocol are not fully utilized for simultaneous transmission and reflection of signals. Besides, it is found that the user U_r has better outage performance than user U_t since the former has smaller path loss than the latter considering the distance $d_r < d_t$.

Fig. 5 gives the ADEP of the warden versus the transmit power for different numbers of STAR-RIS, where the fixed detection threshold τ=-65dBm and optimal threshold (i.e.,(43)) are compared, M=32, 64. From Fig. 5, we can observe that the warden Willie with optimal threshold can obtain lower ADEP than that with fixed threshold. The results indicate that the presented optimal threshold is valid for decreasing the ADEP. Moreover, the system with M=64 has lower ADEP than that with M=32 because larger number of STAR-RIS elements is employed. Besides, the theoretical ADEP can agree with the corresponding simulation, the asymptotic ADEP at high power tends to be the same fixed value and is not related to the M, which accords with the asymptotic analysis at high power in section IV-B. The results above illustrate that the presented theoretical analysis of ADEP is valid for the performance evaluation.

Fig. 6 examines the effect of detection threshold τ on the ADEP, where the transmit power is set as 25dBm and 30dBm,

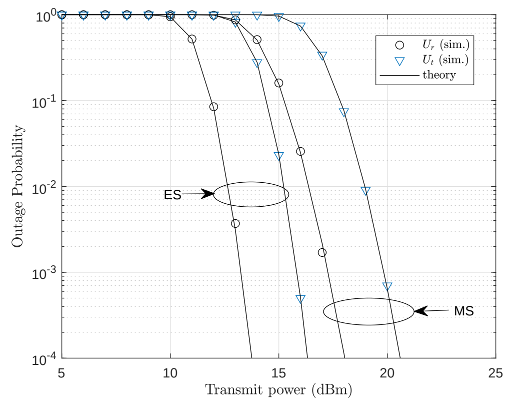

Fig. 4. OP of users versus transmit power for different operating protocols.

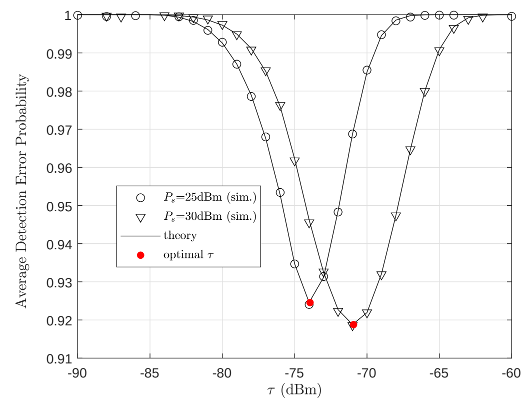

Fig. 6. ADEP versus detection threshold τ for different transmit power.

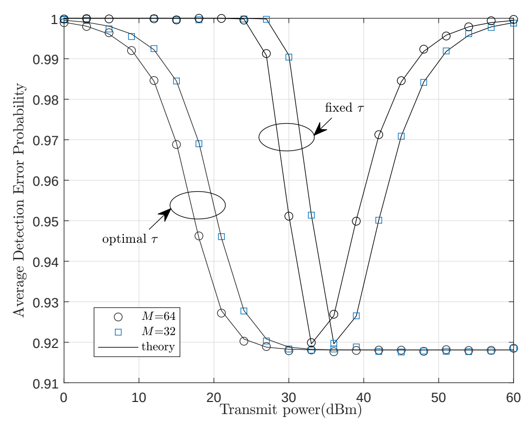

Fig. 5. ADEP versus transmit power for different values of M.

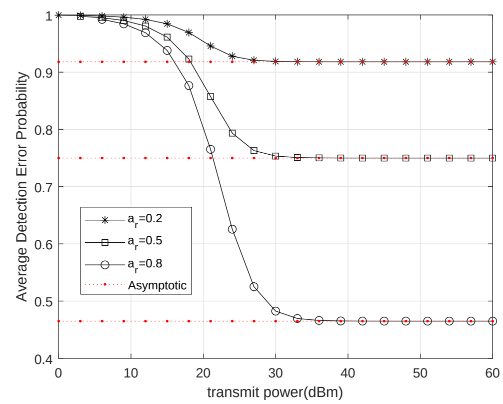

Fig. 7. ADEP versus the transmit power for different values of a_r.

respectively. As shown in Fig. 6, the ADEP first decreases as τ increases, achieving an optimal value, and then increases. Besides, by performing one-dimensional search for τ over the effective range, the lowest ADEP can also be obtained, which is consistent with the theoretical optimal ADEP (marked by 'red' in Fig. 6) achieved by the (49), and correspondingly, the searched optimal τ is also the same as the theoretical τ^o achieved by the (43). Moreover, due to larger transmit power, the system with P_s=30dBm has lower ADEP than that with P_s=25dBm. The above results further illustrate the validity of the proposed optimal detection threshold.

Fig. 7 shows the ADEP of the warden versus the transmit power for different values of the PA coefficient a_r, where the optimal threshold (i.e.,(43)) and asymptotic ADEP (i.e.,(58)) are considered, a_r=0.2, 0.5, 0.8. From Fig. 7, it is found that the ADEP will be small as the PA coefficient a_r increases. The reason is that with the increase of covert user's power, the private information will be easily detected. Hence, we need to control the PA coefficient of covert user for improving the covertness. Besides, the asymptotic ADEP is also consistent with the theoretical ADEP at high power, and it is only related to a_r and decreases with the increase of a_r, which accords with the conclusions in Lemma 4. Thus, the derived asymptotic ADEP is also effective.

In Fig. 8, we plot the ADEP of the warden versus the PA coefficient a_r for different noise powers σ_w^2, where transmit power is 30dBm, the two random noise powers, i.e., noise power1 with η^u =-75dBm, and noise power2 with η^u =-70dBm, as well as the fixed noise power σ_w^2=-80dbm are compared. As shown in Fig. 8, due to the uncertainty of noise power at warden, the system with random noise powers has higher ADEP than that with the fixed power, as expected. Moreover, with the increase of upper bound of random noise power η^u, the ADEP becomes higher as well, i.e., the ADEP with noise power2 is higher than that with noise power1, since the chance of the warden obtaining larger noise power is increased. Thus, the detection performance becomes worse. Besides, the conclusion similar to Fig. 7 can be drawn, i.e, the ADEP becomes lower with the increase of a_r. This is because under this case, the private information of covert user can be easily detected due to larger power allocation.

Fig. 9 illustrates the OP of covert user U_r versus the transmit power, where optimal PA (OPA) scheme based on 2D search and suboptimal PA (SPA) scheme based on 1D search are compared. Meanwhile, to evaluate the effectiveness of the proposed schemes, the fixed PA (FPA) scheme $a_c = 0.6$, $a_t = a_r = 0.2$ is also compared. From Fig. 9, it is found that the proposed two schemes can obtain lower OP than the conventional fixed PA scheme. This is because the latter uses

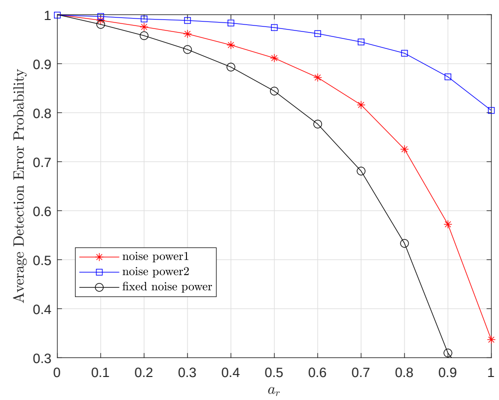

Fig. 8. ADEP versus the power allocation coefficient a_r.

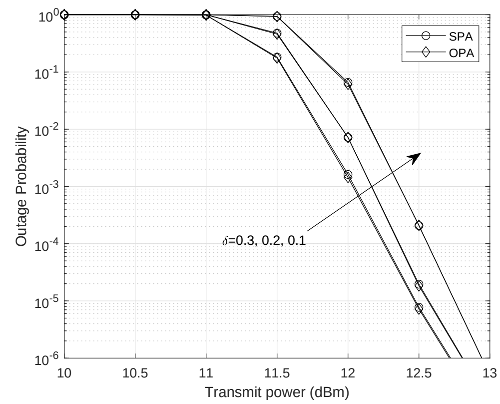

Fig. 10. OP of user U_r versus transmit power for different different values of δ.

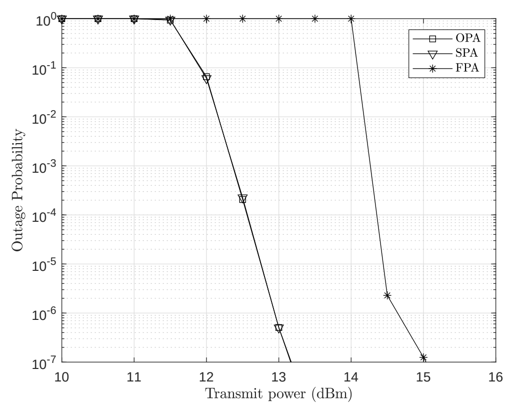

Fig. 9. OP of user U_r versus transmit power for different PA schemes.

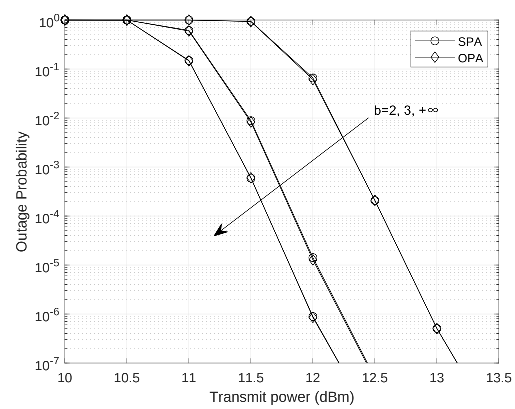

Fig. 11. OP of user U_r versus transmit power for different quantization bit numbers.

the fixed power allocation coefficients and cannot adapt to the change of the system parameters. Moreover, the suboptimal scheme has the outage performance close to the optimal scheme, but the complexity of the former is lower than that of the latter. This is because only 1D search is needed and the search efficiency is higher, which can also be seen from the run time, i.e., the optimal scheme needs about 5.324s, while the suboptimal scheme only needs about 0.031s. The computer used is Intel(R) Core(TM) i9-13900H @ 2.60 GHz.

In Fig. 10, we plot the OP of covert user U_r with the proposed PA schemes for different values of the predefined outage probability δ, where the impact of the δ on the outage performance is evaluated, and δ=0.1, 0.2, 0.3. As illustrated in Fig. 10, the OP of user decreases with the increase of δ. Namely, the OP with δ=0.2 is lower than that with δ=0.1, and the OP with δ=0.3 is lower than that with δ=0.2. This is due to the fact that δ is a limitation on the OP of user Carl U_t. When δ becomes larger, this limitation will be lower. In other words, the constraint condition C_1 in (61) becomes easier to meet. Thus, more PA coefficients $\{a_c, a_r, a_t\}$ satisfying the constraint conditions can be found. As a result, the outage event will not become easier to occur, and corresponding OP will become smaller. Besides, the OPA and SPA schemes still achieve almost the same performances.

In Fig. 11, we evaluate the impact of quantization bit number b on the outage performance of covert user U_r based on the proposed PA schemes, where $b = 2, 3, +\infty$. From Fig. 11, it is found that the outage performance of user is effectively increased with the increase of quantization bit number b. Namely, the user under $b = 3$ has lower OP than that under $b = 2$. This is because the phase errors become smaller as b increases. Besides, the user in the presence of no phase errors ($b = +\infty$) has lower OP than that in the presence of phase errors ($b = 2, 3$), as expected. Furthermore, the presented two schemes are still valid for different quantization bit numbers, and they have almost the same performances.

Fig. 12 illustrates the optimized OP of covert user U_r with different values of fading parameters α and μ, where the suboptimal PA scheme is considered, $\alpha = 1.5, 2.5$, and $\mu = 2, 3$. As shown in Fig. 12, with the increase of fading parameters α and μ, the outage performance is also effectively increased because of better channel fading case. Namely, for the same $\alpha = 2.5$, the user U_r with $\mu = 3$ has lower OP than that with $\mu = 2$, and for the same $\mu = 2$, the user U_r with $\alpha = 2.5$ has lower OP than that with $\alpha = 1.5$. Furthermore, by comparison, it is found that the impact of α on the performance is relatively more obvious than that of μ.

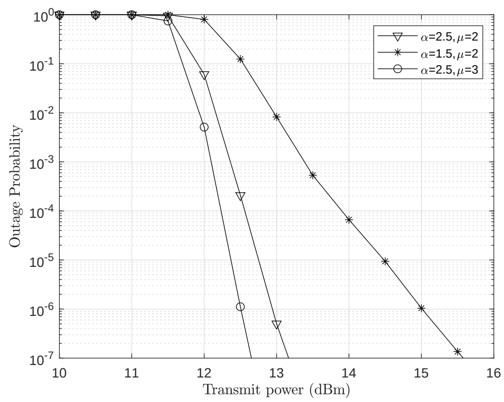

Fig. 12. OP of user U_r versus transmit power for different values of α and μ.

VII. Conclusion

We have studied the covert performance of STAR-RIS aided THz-RSMA systems with phase errors over the α-μ fading channel. Taking the effect of discrete phase errors and generalized α-μ fading into account, the CDF and PDF of the channel gain are respectively derived for the performance analysis. With these results, the OPs of two legitimate users are respectively deduced, and resultant closed-form expressions are obtained. Meanwhile, considering that the noise power obeys a uniform random distribution, the ADEP is derived for the performance evaluation and optimization. Based on this, the optimal detection threshold is also deduced by minimizing the ADEP. As a result, closed-form optimal threshold and ADEP are respectively attained. By analyzing the asymptotic ADEP at high power, it is interestingly found that the obtained asymptotic ADEP is only related to the PA coefficient of covert user Bob, and is also a decreasing function on this PA coefficient. For this reason, we can adjust this PA coefficient to improve the covert performance. Besides, by randomizing the noise power at warden, the covert performance can also been effectively enhanced. Subject to the constraints of the target OP and covertness, the PA coefficients are deduced to minimize the OP of the covert user, and an optimal PA scheme based on 2D search method is proposed to achieve the solution. Furthermore, to lower the complexity, a suboptimal PA scheme based on 1D search method is also presented, it has lower complexity than the optimal scheme because only 1D search is required. Simulation results show the accuracy of the derived theoretical formulae and the validity of the proposed optimization algorithms. In the future work, we will consider the impact of the transceiver hardware impairment (HI) and imperfect SIC, and investigate the covert and outage performances of STAR-RIS aided THz-RSMA systems in the presence of HI and imperfect SIC to improve the practicability. Based on these results, the PA scheme will be developed to increase the corresponding system performances.

Appendix A

In this appendix, we give the derivation of (20). According to [28], for $\alpha-\mu$ fading channel, the expectation and variance of $g_u = |\tilde{h}_{u,m}||\tilde{h}_{ar,m}|$ can be respectively derived as

$$\Omega_u = \mathbb{E}\left(g_u\right) = \mathbb{E}\left(|\tilde{h}_{u,m}||\tilde{h}_{ar,m}|\right) = \hat{h}_f^2, \tag{69}$$

and

$$\begin{aligned} V_u &= \mathbb{D}\left(g_u\right) = \mathbb{E}(g_u^2) - \mathbb{E}^2(g_u) \\ &= \mathbb{E}\left(|\tilde{h}_{u,m}|^2\right)\mathbb{E}\left(|\tilde{h}_{ar,m}|^2\right) - \mathbb{E}^2\left(|\tilde{h}_{u,m}|\right)\mathbb{E}^2\left(|\tilde{h}_{ar,m}|\right) \\ &= \left(\frac{\Gamma^2(\mu)\Gamma^2(\mu+2/\alpha)}{\Gamma^4(\mu+1/\alpha)} - 1\right)\hat{h}_f^4, \end{aligned} \tag{70}$$

where $u \in \{w, t, r\}$.

Let $\Phi_{k,m} = |\tilde{h}_{k,m}||\tilde{h}_{ar,m}|\cos(\bar{\varphi}_{k,m})$ and $\Psi_{k,m} = |\tilde{h}_{k,m}||\tilde{h}_{ar,m}|\sin(\bar{\varphi}_{k,m})$, considering $\bar{\varphi}_{k,m} \sim \mathrm{U}(-\upsilon\pi, \upsilon\pi)$, then we calculate the expectation and variance of Φ as

$$\begin{aligned} \mathbb{E}(\Phi_{k,m}) &= \mathbb{E}(g_k)\mathbb{E}\left(\cos(\bar{\varphi}_{k,m})\right) \\ &= \Omega_k \sin c(\upsilon\pi) = \bar{\Phi}_k, \end{aligned} \tag{71}$$

and

$$\begin{aligned} \mathbb{D}(\Phi_{k,m}) &= \mathbb{E}\left(g_k\cos(\bar{\varphi}_{k,m})\right)^2 - \left(\mathbb{E}(g_k)\mathbb{E}(\cos(\bar{\varphi}_{k,m}))\right)^2 \\ &= (V_k + \Omega_k^2)\tfrac{1+\sin c(2\upsilon\pi)}{2} - \Omega_k^2 \sin c^2(\upsilon\pi) = V_{\Phi,k}, \end{aligned} \tag{72}$$

where $\mathbb{E}\left(\sin(\bar{\varphi}_{k,m})\right)$=0, $\mathbb{D}\left(\sin(\bar{\varphi}_{k,m})\right)$=$[1-\sin c(2\upsilon\pi)]/2$, $\mathbb{D}\left(\cos\left(\bar{\varphi}_{k,m}\right)\right)$ =$\frac{1+\sin c(2\upsilon\pi)}{2} - \sin c^2(\upsilon\pi)$, and $\mathbb{E}\left(\cos(\bar{\varphi}_{k,m})\right)$ =$\sin c(\upsilon\pi)$ are utilized. The function $\sin c(x)$=$\frac{\sin(x)}{x}$.

Similarly, the expectation and variance of Ψ can be respectively derived as

$$\begin{aligned} &\mathbb{E}\left(\Psi_{k,m}\right) = 0, \\ \text{and } &\mathbb{D}\left(\Psi_{k,m}\right) = (V_k + \Omega_k^2)\tfrac{1-\sin c(2\upsilon\pi)}{2} = V_{\Psi,k}. \end{aligned} \tag{73}$$

In terms of (18), we have: $T_k = \sum_{m=1}^{M}\Phi_{k,m}$, and $W_k = \sum_{m=1}^{M}\Psi_{k,m}$. Considering that M is very large in general, according to the CLT, T_k and W_k will tend to the Gaussian distributions as $T_k \sim \mathcal{N}\left(M\bar{\Phi}_k, MV_{\Phi,k}\right)$ and $W_k \sim \mathcal{N}\left(0, MV_{\Psi,k}\right)$. Based on this, $\frac{T_k^2}{MV_{\Phi,k}}$ will obey the non-central chi-square distribution with one degree of freedom and non-central parameter $\lambda_k = \frac{M\hat{h}_f^4 \sin c^2(\upsilon\pi)}{V_{\Phi,k}}$, and $\frac{W_k^2}{MV_{\Psi,k}}$ obeys the central chi-square distribution with one degree of freedom. In terms of the expectation and variance of the non-central chi-square distribution [39], we can derive the expectation and variance of T_k^2 as

$$\begin{aligned} \mathbb{E}\left(T_k^2\right) &= MV_{\Phi,k}(1+\lambda_k), \\ \mathbb{D}\left(T_k^2\right) &= 2(MV_{\Phi,k})^2(1+2\lambda_k), \end{aligned} \tag{74}$$

and the expectation and variance of W_k^2 as

$$\mathbb{E}\left(W_k^2\right) = MV_{\Psi,k},\ \ \mathbb{D}\left(W_k^2\right) = 2(MV_{\Psi,k})^2. \tag{75}$$

In terms of (18), $Z_k = T_k^2 + W_k^2$. Hence, we can calculate two parameters $\mathcal{O}_k = \frac{\{\mathbb{E}(Z_k)\}^2}{\mathbb{D}(Z_k)}$ and $\mathcal{C}_k = \frac{\mathbb{E}(Z_k)}{\mathbb{D}(Z_k)}$ as (20), i.e.,

$$\begin{aligned} &\mathcal{O}_k = \tfrac{(MV_{\Phi,k}(1+\lambda_k)+MV_{\Psi,k})^2}{2(MV_{\Phi,k})^2(1+2\lambda_k)+2(MV_{\Psi,k})^2} \\ \text{and } &\mathcal{C}_k = \tfrac{MV_{\Phi,k}(1+\lambda_k)+MV_{\Psi,k}}{2(MV_{\Phi,k})^2(1+2\lambda_k)+2(MV_{\Psi,k})^2}. \end{aligned} \tag{76}$$

Appendix B

In this appendix, we give the derivation of Eq. (33).

As shown in (32), X_w can be re-expressed as

$$\begin{aligned} X_w = &\left|\sum_{m=1}^{M} |\tilde{h}_{w,m}||\tilde{h}_{ar,m}|\cos(\varphi_{w,m})\right|^2 \\ &+ \left|\sum_{m=1}^{M} |\tilde{h}_{w,m}||\tilde{h}_{ar,m}|\sin(\varphi_{w,m})\right|^2 \\ = &\left(\sum_{m=1}^{M} \Re_{w,m}\right)^2 + \left(\sum_{m=1}^{M} \Im_{w,m}\right)^2, \end{aligned} \tag{77}$$

where $\Re_{w,m} = |\tilde{h}_{w,m}||\tilde{h}_{ar,m}|\cos(\varphi_{w,m})$ and $\Im_{w,m} = |\tilde{h}_{w,m}||\tilde{h}_{ar,m}|\sin(\varphi_{w,m})$. Considering that $\varphi_{w,m}$ obeys a uniform distribution over $[0, 2\pi]$, the expectation and variance of the real part $\Re_{w,m}$ and imaginary part $\Im_{w,m}$ are respectively given by

$$\mathbb{E}(\Re_{w,m}) = \mathbb{E}\left(|\tilde{h}_{w,m}||\tilde{h}_{ar,m}|\right)\mathbb{E}\left(\cos(\varphi_{w,m})\right) = 0, \tag{78}$$

$$\begin{aligned} \mathbb{D}(\Re_{w,m}) = &\mathbb{E}\left((|\tilde{h}_{w,m}||\tilde{h}_{ar,m}|)^2\right)\mathbb{E}\left(\cos^2\varphi_{w,m}\right) \\ &- \left(\mathbb{E}(|\tilde{h}_{w,m}||\tilde{h}_{ar,m}|)\mathbb{E}(\cos(\varphi_{w,m}))\right)^2 \\ = &\frac{V_w+\Omega_w^2}{2} = \frac{\Gamma^2(\mu)\Gamma^2(\mu+2/\alpha)}{2\Gamma^4(\mu+1/\alpha)}\hat{h}_f^4, \end{aligned} \tag{79}$$

and

$$\mathbb{E}(\Im_{w,m}) = \mathbb{E}\left(|\tilde{h}_{w,m}||\tilde{h}_{ar,m}|\right)\mathbb{E}\left(\sin(\varphi_{w,m})\right) = 0, \tag{80}$$

$$\begin{aligned} \mathbb{D}(\Im_{w,m}) = &\mathbb{E}\left((|\tilde{h}_{w,m}||\tilde{h}_{ar,m}|)^2\right)\mathbb{E}\left(\sin^2\varphi_{w,m}\right) \\ &- \left(\mathbb{E}(|\tilde{h}_{w,m}||\tilde{h}_{ar,m}|)\mathbb{E}(\sin(\varphi_{w,m}))\right)^2 \\ = &\frac{V_w+\Omega_w^2}{2} = \frac{\Gamma^2(\mu)\Gamma^2(\mu+2/\alpha)}{2\Gamma^4(\mu+1/\alpha)}\hat{h}_f^4. \end{aligned} \tag{81}$$

Let $Q_w = \sum_{m=1}^{M} \Re_{w,m}$, and $S_w = \sum_{m=1}^{M} \Im_{w,m}$, then $X_w = Q_w^2 + S_w^2$. Considering M is very large in general, according to the CLT, Q_w and S_w will tend to the Gaussian distributions as $Q_w \sim \mathcal{N}\left(0, M\frac{V_w+\Omega_w^2}{2}\right)$ and $S_w \sim \mathcal{N}\left(0, M\frac{V_w+\Omega_w^2}{2}\right)$. Thus, $\frac{Q_w^2+S_w^2}{M(V_w+\Omega_w^2)/2}$ obeys the central chi-square distribution with 2 degrees of freedom. Based on this, using (75), we can calculate that $\mathbb{E}(X_w) = \mathbb{E}(Q_w^2) + \mathbb{E}(S_w^2) = M(V_w + \Omega_w^2)$ and $\mathbb{D}\left(X_w\right) = \mathbb{D}(Q_w^2) + \mathbb{D}(S_w^2) = M^2\left(V_w + \Omega_w^2\right)^2$. Since the chi-square distribution can be transformed into a gamma distribution, then we have: $X_w \sim \Gamma\left(\iota_w, o_w\right)$, where the shape parameter $\iota_w = \frac{(\mathbb{E}(X_w))^2}{\mathbb{D}(X_w)} = 1$ and the rate parameter $o_w = \frac{\mathbb{E}(X_w)}{\mathbb{D}(X_w)} = \frac{1}{M(V_w+\Omega_w^2)}$. Correspondingly, the PDF of X_w is approximately given by

$$f_{X_w}(x) \simeq o_w e^{-o_w x}. \tag{82}$$

Under this case, the gamma distribution is reduced to an exponential distribution with parameter $\theta_w = \frac{1}{o_w} = M\frac{\Gamma^2(\mu)\Gamma^2(\mu+2/\alpha)}{2\Gamma^4(\mu+1/\alpha)}\hat{h}_f^4$. Correspondingly, the PDF of X_w is changed to

$$f_{X_w}(x) \simeq (1/\theta_w)e^{-x/\theta_w}. \tag{83}$$

References

[1] K. Tekbiyik, A. R. Ekti, G. K. Kurt, A. Gorcin and H. Yanikomeroglu, "A holistic investigation of terahertz propagation and channel modeling toward vertical heterogeneous networks," *IEEE Commun. Mag.*, vol. 58, no. 11, pp. 14-20, Nov. 2020.

[2] J. Xu, C. Yuen, C. Huang, N. Ul Hassan, G. C. Alexandropoulos, M. D. Renzo, M. Debbah, "Reconfiguring wireless environments via intelligent surfaces for 6G: Reflection, modulation, and security," *Sci. China Inf. Sci*, vol.66, 130304:1-20, Feb. 2023.

[3] G. C. Alexandropoulos, K, D. Katsanos, M. Wen, D. B. D. Costa, "Counteracting eavesdropper attacks through reconfigurable intelligent surfaces: A new threat model and secrecy rate optimization," *IEEE Open J. Commun. Soc*, vol. 4, pp. 1285-1302, 2023.

[4] A. M. T. Khel and K. A. Hamdi, "Analytical performance evaluation of STAR-RIS assisted terahertz wireless communications," *IEEE Trans. Veh. Technol.*, vol. 73, no. 4, pp. 5500-5515, Apr. 2024.

[5] X. Mu, Y. Liu, L. Guo, J. Lin, and R. Schober,"Simultaneously transmitting and reflecting (STAR) RIS aided wireless Communications," *IEEE Trans. Wireless Commun.*, vol.21, no. 5, pp. 3083-3098, May, 2022.

[6] Y. Mao, O. Dizdar, B. Clerckx, R. Schober, P. Popovski and H. V. Poor, "Rate-splitting multiple access: Fundamentals, survey, and future research trends," *IEEE Commun. Surv. Tutorials*, vol. 24, no. 4, pp. 2073-2126, 2022.

[7] Z. Li, T. Rahim, P. Xiao, J. Si, S. Yan, Q. Ni, "Intelligent covert communication," *China Commun..*, vol. 21, no. 9, pp.3-5, 2024

[8] F. Naeem, M. Ali, G. Kaddoum, C. Huang, C. Yuen, "Security and privacy for reconfigurable intelligent surface in 6G: a review of prospective applications and challenges," *IEEE Open J. Comm. Soc.*, vol. 4, pp. 1196-1217, May 2023.

[9] X. Lu, E. Hossain, T. Shafique, S. Feng, H. Jiang and D. Niyato, "Intelligent reflecting surface enabled covert communications in wireless networks," *IEEE Netw.*, vol. 34, no. 5, pp. 148-155, Sep./Oct. 2020.

[10] R. Kaur, B. Bansal, S. Majhi, S. Jain, C. Huang, C. Yuen, "A survey on reconfigurable intelligent surface for physical layer security of next-generation wireless communications," *IEEE Open J. Veh. Technol.*, vol.5, 172-199, Jan 2024.

[11] K. D. Katsanos, and G. C. Alexandropoulos, "Spatial secrecy spectral efficiency optimization enabled by reconfigurable intelligent surfaces," in *Proc. 2023 31st European Signal Processing Conference (EUSIPCO'2023)*, Helsinki, Finland, 2023, pp. 1539-1543.

[12] G. C. Alexandropoulos, K. Katsanos, M. Wen, and D. B. D. Costa,"Safeguarding MIMO communications with reconfigurable metasurfaces and artificial noise," *Proc. IEEE International Conference on Communications (ICC'2021)*, Montreal, Canada, 2021, pp. 1-6.

[13] G. Rexhepi, H. S. Rou, G. T. F. d. Abreu, and G. C. Alexandropoulos, "Blinding the wiretapper: RIS-enabled user occultation in the ISAC era," Available: https://arxiv.org/abs/2504.15033.

[14] J. Zhang, W. Wang, Y. Gao, W. Lu, N. Zhao and D. Niyato, "Robust covert multicasting aided by STAR-RIS with hardware impairment," *IEEE Trans. Wireless Commun.*, vol. 23, no. 11, pp. 16172-16186, Nov. 2024.

[15] H. Xiao, X. Hu, P. Mu, W. Wang, T.-X. Zheng, K.-K. Wong, K. Yang, "Simultaneously transmitting and reflecting RIS (STAR-RIS) assisted multi-antenna covert communication: analysis and optimization," *IEEE Trans. Wireless Commun.*, vol. 23, no. 6, pp. 6438-6452, June 2024.

[16] X. Li, J, Zhao, G, Chen, W. Hao, D. B. D. Costa, A. Nallanathan, H. Shin, and C. Yuen,"STAR-RIS assisted covert wireless communications with randomly distributed blockages," *IEEE Trans. Wireless Commun.*, Early Access. 2025.

[17] X. Li, Z. Tian, W. He, G. Chen, M. C. Gursoy, S. Mumtaz, A. Nallanathan, "Covert communication of STAR-RIS aided NOMA networks," *IEEE Trans. Veh. Technol.*, vol. 73, no. 6, pp. 9055-9060, Jun. 2024.

[18] Q. Li, D. Xu, K. Zhang, K. Navaie and Z. Ding, "Covert communications in STAR-RIS assisted NOMA IoT networks over Nakagami-m fading channels," *IEEE Internet Things J.*, vol. 11, no. 12, pp. 22456-22470, Jun. 2024.

[19] Y. Liang, L. Yang, I. Ahmad, M, Valkama, "Covert transmission and physical-layer security of STAR-RIS-assisted uplink SGF-NOMA systems," *IEEE Trans. Commun.*, Early Access. 2025.

[20] J. Zhang, X. Li, P. Guo, W. Hao, L. Yang, H. Deng, G. Nie, "STAR-RIS enabled RSMA-intelligent autonomous transport system: joint security and covertness analysis," *IEEE Trans. Intell. Transp. Syst.*, Early Access, 2025.

[21] Y. Zhang, L. Yang, X. Li, K. Guo and H. Liu, "Covert communications for STAR-RIS-assisted industrial networks with a full duplex receiver and RSMA," *IEEE Internet Things J.*, vol. 11, no. 12, pp. 22483-22493, 15 Jun. 15, 2024.

[22] L. Yang, Z. Zhang, S. Du, "Covert communication for STAR-RIS-assisted ambient backscatter communication systems with RSMA," *IEEE Trans. Cogn. Commun. and Netw.*, Early Access. 2025.

[23] Y. Liang, K. Huang, L. Yang, X. Li, H. Liu and Y. Bian, "Covert communications for active STAR-RIS-aided RSMA systems with hardware impairments," *IEEE Trans. Intell. Transp. Syst.*, vol. 26, no.7, pp. 10036-10047, 2025.

[24] M. Tatar Mamaghani and Y. Hong, "Aerial intelligent reflecting surface-enabled terahertz covert communications in beyond-5G internet of things," *IEEE Internet Things J.*, vol. 9, no. 19, pp. 19012-19033, Oct. 1, 2022.

[25] W. Gao, Y. Chen, C. Han and Z. Chen, "Distance-adaptive absorption peak modulation (DA-APM) for terahertz covert communications," *IEEE Trans. Wireless Commun.*, vol. 20, no. 3, pp. 2064-2077, Mar. 2021.

[26] Z. Zhakipov, K. M. Rabie, X. Li and G. Nauryzbayev, "Accurate approximation to channel distributions of cascaded RIS-aided systems with phase errors over Nakagami-m Channels," *IEEE Wireless Commun. Lett.*, vol. 12, no. 5, pp. 922-926, 2023.

[27] S. Zhou, W. Xu, K. Wang, M. Di Renzo and M. -S. Alouini, "Spectral and energy efficiency of IRS-assisted MISO communication with hardware impairments," *IEEE Wireless Commun. Lett.*, vol. 9, no. 9, pp. 1366-1369, 2020.

[28] M. D. Yacoub, "The α-μ distribution: a physical fading model for the stacy distribution," *IEEE Trans. Veh. Technol.*, vol. 56, no. 1, pp. 27-34, 2007.

[29] E. N. Papasotiriou, A.-A. A. Boulogeorgos, K. Haneda, M. F. de Guzman, and A. Alexiou, "An experimentally validated fading model for THz wireless systems" *Sci. Rep.*, vol. 11, no. 1, pp. 1-14, Sep. 2021.

[30] I. S. Gradshteyn and I. M. Ryzhik, *Table of integrals, series, and products*. Academic press, 2007.

[31] C. Wu, Y. Liu, X. Mu, X. Gu and O. A. Dobre, "Coverage characterization of STAR-RIS networks: NOMA and OMA," *IEEE Commun. Lett.*,vol. 25, no. 9, pp. 3036-3040, 2021.

[32] R. Hashemi, S. Ali, N. H. Mahmood and M. Latva-aho, "Average rate and error probability analysis in short packet communications over RIS-aided URLLC systems," *IEEE Trans. Veh. Technol.*, vol. 70, no. 10, pp. 10320-10334, 2021.

[33] P. Ren, J. Zhang, S. Yan, W. Xu, J. Sun and N. Al-Dhahir, "Covert communications assisted by reconfigurable intelligent surfaces with discrete phase shifts," in *Proc. 2023 IEEE Global Communications Conference(GLOBECOM)*, Kuala Lumpur, Malaysia, 2023, pp. 4859-4864.

[34] T. V. Sobers, B. A. Bash, S. Guha, D. Towsley, and D. Goeckel, "Covert communication in the presence of an uninformed jammer," *IEEE Trans. Wireless Commun.*, vol. 16, no. 9, pp. 6193-6206, Sep. 2017.

[35] Y. Su, H. Sun, Z. Zhang, Z. Lian, Z. Xie and Y. Wang, "Covert communication with relay selection," *IEEE Wireless Commun. Lett.*, vol. 10, no. 2, pp. 421-425, Feb. 2021.

[36] Y. Cheng, Z. Xiong, Z. Wang, D. Niyato, W. Y. B. Lim and B. Li, "Performance analysis of jammer-assisted covert rate-splitting multiple access," in *Proc. IEEE/CIC International Conference on Communications in China (ICCC)*, Hangzhou, China, 2024, pp. 915-920.

[37] H.-M. Wang, Y. Zhang, X. Zhang, and Z. Li, "Secrecy and covert communications against uav surveillance via multi-hop networks," *IEEE Trans. Commun.*, vol. 68, no. 1, pp. 389-401, Jan. 2020.

[38] J. Hu, S. Yan, F. Shu, and J. Wang, "Covert transmission with a self-sustained relay,"*IEEE Trans. Wireless Commun.*, vol. 18, no. 8, pp. 4089-4102, Aug. 2019.

[39] N. P. Le and M. -S. Alouini, "Performance analysis of RIS-aided THz wireless systems over $\alpha - \mu$ fading: an approximate closed-form approach," *IEEE Internet Things J.*, vol. 11, no. 1, pp. 1328-1343, Jan. 2024.

[40] T. L. Nguyen, T. N. Do, G. Kaddoum, D. B. d. Costa and Z. J. Haas, "Channel characterization for RIS-aided terahertz communications: A stochastic approach," *IEEE Wireless Commun. Lett.*, vol. 11, no. 9, pp. 1890-1894, Sep. 2022.

[41] L. Li, Z. Chen, R. Chen, L. Yang and S. Yan, "Covert wireless communication with random frequency diverse array," *IEEE Trans. Veh. Technol.*, vol. 73, no. 1, pp. 1473-1478, Jan. 2024.

[42] X. Mu, Y. Liu, L. Guo, J. Lin and R. Schober, "Simultane ously transmitting and reflecting (STAR) RIS aidedwireless communications," *IEEE Trans. Wireless Commun.*,, vol.21, no. 5, pp.3083-3398, May 2022.